

# Chemistry of mixed nitrogen- and sulfur-donor tridentate macrocycles

Jonathan P. Danks, Neil R. Champness, Martin Schröder \*

*Department of Chemistry, The University of Nottingham, Nottingham, NG7 2RD, UK*

Received 16 January 1998; accepted 16 March 1998

## Contents

Abstract	417
1. Introduction	418
2. Ligand synthesis	418
3. Stability constants and kinetic properties	420
4. Metal complexes of [9]aneN <sub>2</sub> S, [10]aneN <sub>2</sub> S, [9]aneNS <sub>2</sub> and [10]aneNS <sub>2</sub>	424
4.1. Vanadium	424
4.2. Molybdenum and tungsten	424
4.3. Manganese and rhenium	427
4.4. Iron and ruthenium	428
4.5. Cobalt and rhodium	429
4.6. Nickel	431
4.7. Palladium and platinum	435
4.8. Copper	440
4.9. Silver and gold	443
4.10. Zinc and mercury	445
4.11. Indium, thallium and lead	446
5. N-Functionalised tridentate mixed-donor nitrogen and sulfur macrocycles	448
6. S-Functionalised tridentate mixed-donor nitrogen and sulfur macrocycles	463
7. Concluding remarks	466
8. References	466

## Abstract

The synthesis and co-ordination chemistry of tridentate N/S-mixed donor macrocycles is reviewed. © 1998 Elsevier Science S.A. All rights reserved.

**Keywords:** Aza; Complexation; Macrocycle; Metal; Thioether

\* Corresponding author. Tel: 0044-1159515151; Fax: 0044-1159513563; e-mail: m.schroder@nott.ac.uk

## 1. Introduction

Busch was the first to show that thioether macrocyclic ligands effectively bind transition metal ions [1–3]. Since then the chemistry of homoleptic thioether crowns has been developed widely [4–6]. The co-ordination chemistry of mixed nitrogen- and sulfur-donor macrocycles has also been an area of increasing interest over the past 15 years. These ligands are of interest as they offer co-ordination of both hard  $\sigma$ -donor N-ligands and soft  $\sigma$ -donor and potential  $\pi$ -acceptor [7,8] S-ligands. In particular, small ring tridentate macrocyclic ligands such as 1,4,7-triazacyclononane ([9]aneN<sub>3</sub>) and 1,4,7-trithiacyclononane ([9]aneS<sub>3</sub>) (Fig. 1) have been shown to act as highly effective face-capping ligands that co-ordinate readily to metal centres to form highly stable complexes, many of which have unusual co-ordination geometries and oxidation states. These homoleptic macrocycles have been extensively studied and reviews have been published covering the rich co-ordination chemistry they offer [4–6,9]. This review focusses on the synthesis and co-ordination chemistry of the small ring crowns 1,4-diaza-7-thiacyclononane ([9]aneN<sub>2</sub>S) and 1-aza-4,7-dithiacyclononane ([9]aneNS<sub>2</sub>) (Fig. 1)

## 2. Ligand synthesis

The synthesis of 1,4-diaza-7-thiacyclononane, [9]aneN<sub>2</sub>S, was first published [10–12] in the early 1980s using a modified Richman–Atkins preparation [13]. The synthesis of the ditosylated macrocycle has since been improved [14–16]. In the original preparation, two routes to the ditosylated ring precursor were considered

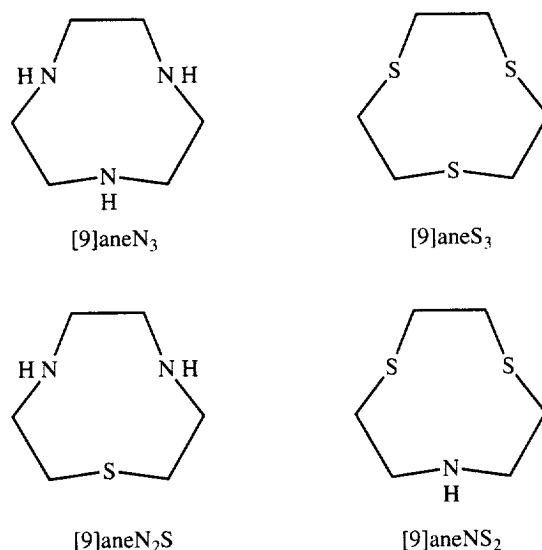
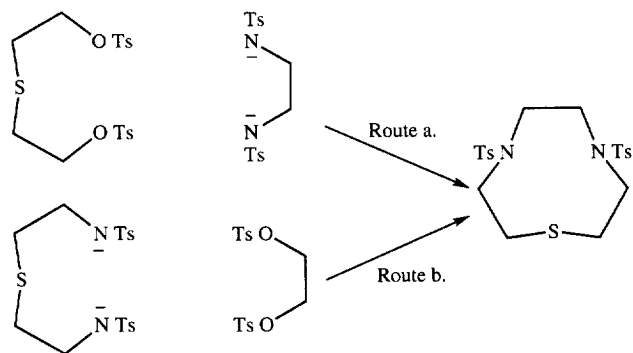
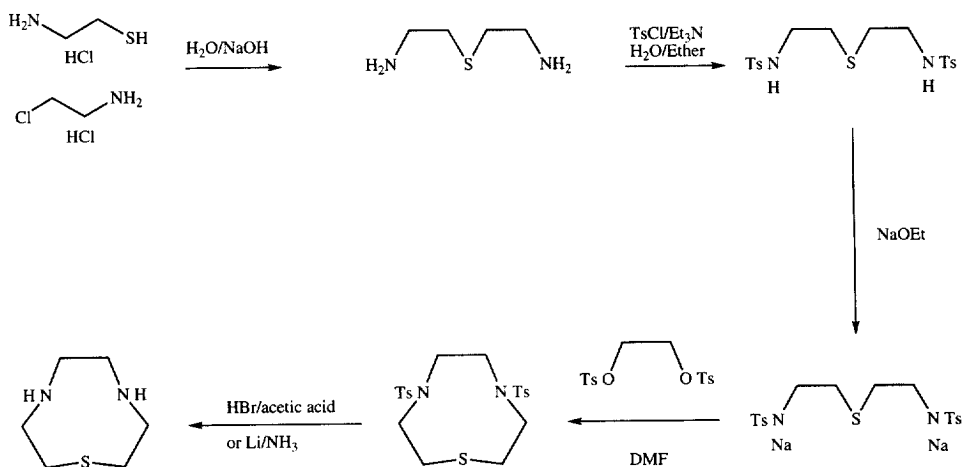


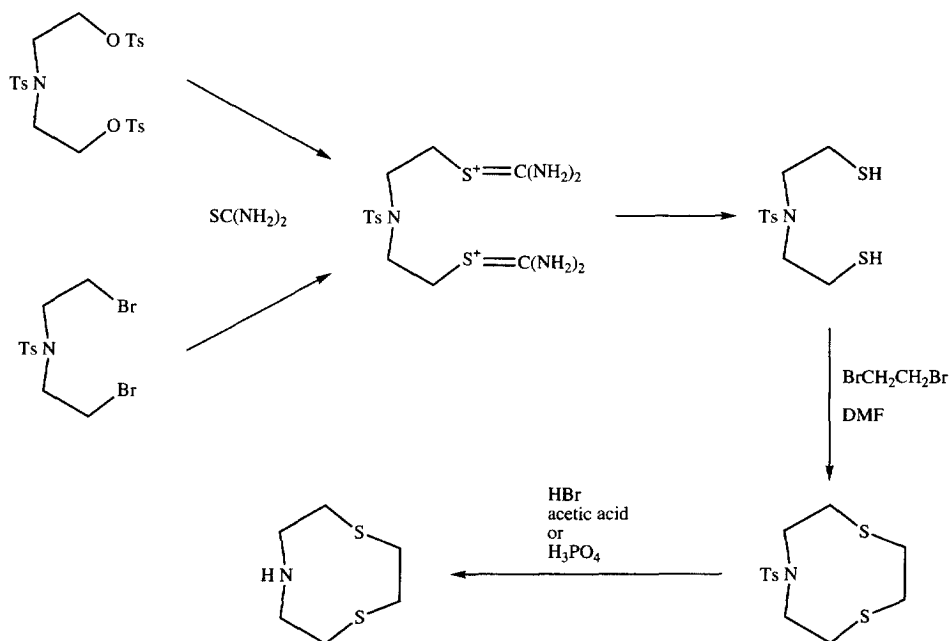
Fig. 1. Nine-membered nitrogen/sulfur macrocyclic ligands.

Scheme 1. Synthesis of  $\text{Ts}_2[9]\text{aneN}_2\text{S}$ .

(Scheme. 1). The first *via* the ditosylate of 2,2'-thiodiethanol (Route a) offered an attractive methodology in terms of synthetic simplicity and cost. However, the authors abandoned it due to the instability to hydrolysis of the ditosylate. Route b was the second and adopted route. The use of  $\text{H}_2\text{SO}_4$  is to be avoided in the final detosylation step due to presumed acid-catalysed C–S bond cleavage and/or oxidation side reactions. A milder acid hydrolysis is generally employed utilising  $\text{HBr}$ /acetic acid. A reductive, alkaline detosylation in *n*-butanol/*di-n*-butyl ether and sodium improves the yield considerably (K. Wieghardt, I. Tolkendorf, unpublished results), while the use of lithium/liquid ammonia also gives excellent results in minutes [16]. The full preparation from commercially available starting materials is shown in Scheme. 2.

The synthesis of 1-aza-4,7-dithiacyclononane,  $[9]\text{aneNS}_2$ , was first reported by both Parker [17] and McAuley [18,19] independently in 1990. Whilst the ring closure step for the synthesis of  $[9]\text{aneN}_3$  and  $[9]\text{aneN}_2\text{S}$  does not require high dilution

Scheme 2. Preparation of  $[9]\text{aneN}_2\text{S}$ .



Scheme 3. Synthesis of [9]aneNS<sub>2</sub>, employed by Parker [17] and McAuley [18].

techniques, this is not true for [9]aneNS<sub>2</sub> or [9]aneS<sub>3</sub>, both of which require the addition of the reactants over several hours into a large volume of solvent. The routes employed by Parker and McAuley (Scheme 3) were essentially the same differing only in the final detosylation step. McAuley reported difficulty in this final step and finally used phosphoric acid to give a 50% yield, while Parker opted for HBr in acetic acid and achieved a reported conversion of 73%. McAuley has since reported [19] the synthesis of [10]aneNS<sub>2</sub> via an alternative route requiring fewer steps (Scheme. 4). This method has been adopted subsequently for the synthesis of [9]aneNS<sub>2</sub> with greatly improved overall yields [20,21].

### 3. Stability constants and kinetic properties

Before dealing with the properties of transition metal complexes of these heteroleptic macrocycles, it is useful to comment upon their acid–base properties in comparison with their open chain-analogues, with [9]aneN<sub>3</sub> and its open-chain analogues.

The stepwise protonation constants for [9]aneN<sub>3</sub> [22–27], diethylenetriamine (deta) [28,29], [9]aneN<sub>2</sub>S [12,30] [10]aneN<sub>2</sub>S [30], and diaminodiethylsulphide (daes) [28] (Fig. 2) are shown in Table 1. For the open-chain analogues (daes) and (deta) the values of pK<sub>1</sub> and pK<sub>2</sub> do not vary greatly as the central donor atom is varied from nitrogen to sulfur. The central atom therefore does not exert appreciable electronic effect upon the primary amine sites. The change in basicity between

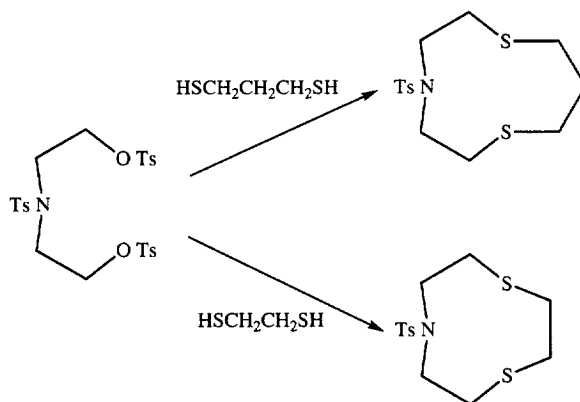
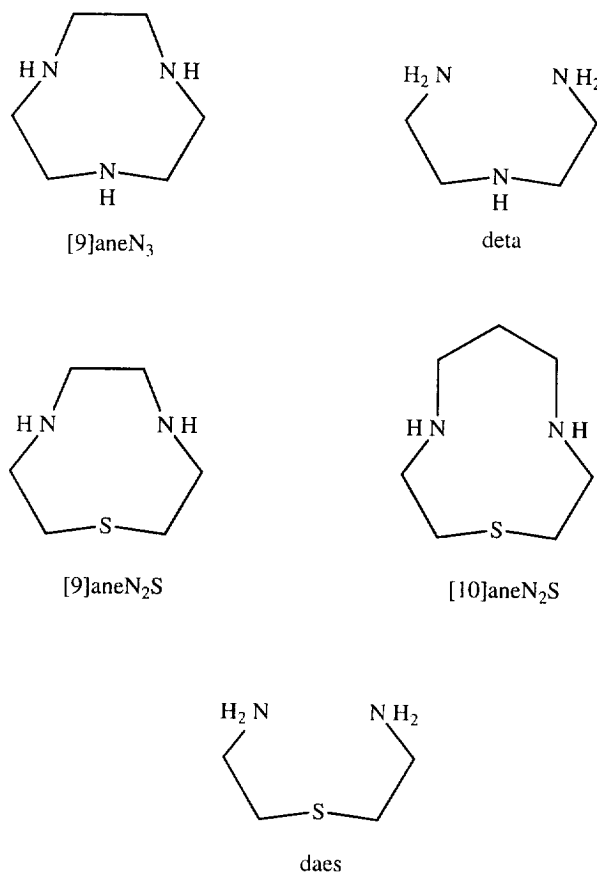
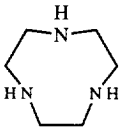
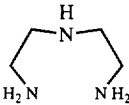
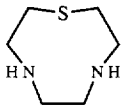
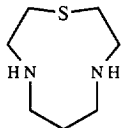
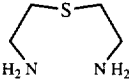
Scheme 4. Synthesis of Ts[9]aneN<sub>2</sub>S and Ts[10]aneNS<sub>2</sub>.

Fig. 2. Nine- and 10-membered nitrogen/sulfur macrocyclic ligands and their open-chain analogues.

Table 1

Stepwise protonation constants for [9]aneN<sub>3</sub>, deta, [9]aneN<sub>2</sub>S, [10]aneN<sub>2</sub>S and daes

		$pK_1$	$pK_2$	$pK_3$	Refs
	[9]aneN <sub>3</sub>	10.42	6.82	Very small	[22]
		10.47	6.80	< 2.5	[23]
		12.60	7.24	Very small	[24]
		10.59	6.88	< 1.0	[25]
		10.68	6.86	2.1	[26]
		10.40	6.90	~0.4 ± 0.2	[27]
	Deta	9.70	8.98	4.25	[28, 29]
	[9]aneN <sub>2</sub> S	9.67	3.92		[12]
		9.89	4.18		[30]
	[10]aneN <sub>2</sub> S	12.0	3.25		[30]
	daes	9.50	8.70		[28]

[9]aneN<sub>3</sub> and [9]aneN<sub>2</sub>S is therefore not an inductive effect but is probably due to the difference of H-bonding ability of the two ligands, [9]aneN<sub>3</sub> being set-up for internal H-bonding between all three N-donors [31]. The stepwise protonation constants for [9]aneN<sub>3</sub> therefore contrast markedly with those of its open-chain derivative (deta). The first protonation constant is higher for [9]aneN<sub>3</sub> than for deta, whereas the values for the second and third protonation constants are significantly lower. This can be rationalised in the following manner. In the free cyclic amine the electron-pairs of the N atoms are directed towards the centre of the ring due to constraints of the ring structure. The electron density at the centre of the ring is therefore enhanced and makes the first protonation more favourable than for the open-chain analogue, deta. As the three nitrogen centres are in close proximity to one another in the macrocyclic ring, electrostatic repulsions between the quaternised nitrogen atom(s) and incoming protons make subsequent protonation less favourable and reduced protonation constants are observed for [9]aneN<sub>3</sub> compared to its open-chain analogue, deta. In contrast, the first protonation constant for

[9]aneN<sub>2</sub>S does not show a significant increase over its open chain analogue (daes). The second protonation for [9]aneN<sub>2</sub>S, however, does show a significant decrease as in [9]aneN<sub>3</sub> and is rationalised in the same manner. The first protonation constant for [10]aneN<sub>2</sub>S is significantly higher than for its nine membered ring analogue and its second is much lower. This cannot be rationalised using electrostatic repulsion arguments as the nitrogen atoms are further separated in [10]aneN<sub>2</sub>S than in [9]aneN<sub>2</sub>S, though it has been reasoned [30] that the formation of an enhanced internal <sup>+</sup>N-H<sup>+</sup>⋯N hydrogen bond accounts for this seemingly anomalous behaviour. To our knowledge, there are no data available for the protonation constant for [9]aneNS<sub>2</sub>.

The formation constants for metal complexation ( $\log K_1$  and  $\log K_2$ ) for [9]aneN<sub>2</sub>S, [10]aneN<sub>2</sub>S and daes are shown in Table 2. Also listed are the values for the  $\log K_{(\text{mac})}$ , which is  $\log K$  for the macrocyclic complex minus the  $\log K$  for the analogous open-chain metal complex. The term  $\log K_{(\text{mac})}$  is therefore a measure of the macrocyclic effect. For all ligands, the order of stability is Co < Ni < Cu > Zn which conforms to the Irving–Williams series. The values of  $\log K_{(\text{mac})}$  show an appreciable increase for the complexes of [9]aneN<sub>2</sub>S over their open-chain analogues. Table 2 also indicates that [10]aneN<sub>2</sub>S forms weaker complexes than [9]aneN<sub>2</sub>S resulting in lower values for their macrocyclic effect. The macrocyclic effect for [9]aneN<sub>2</sub>S and [10]aneN<sub>2</sub>S is, however, smaller than for [9]aneN<sub>3</sub> with the exception for the Cu(II) complex of [9]aneN<sub>3</sub> where  $\log K_{(\text{mac})} = -0.4$ . This reflects the unfavourable effects produced by forcing a N atom of [9]aneN<sub>3</sub> to occupy an axial position at a Jahn–Teller distorted d<sup>9</sup> Cu(II) site. Allowing an S-donor to occupy the axial site appears to accommodate the Jahn–Teller distortion more readily than the axial N-donor in [Cu([9]aneN<sub>3</sub>)<sub>2</sub>]<sup>2+</sup> because of the relatively poorer  $\sigma$ -donating properties of the thioether S-donor.

Table 2

Metal complex formation constants ( $\log K$ ) of [9]aneN<sub>2</sub>S, daes and [10]aneN<sub>2</sub>S at 25 °C and 0.1 M

Refs	[9]aneN <sub>2</sub> S			Daes		$\log K_{(\text{mac})}^a$		[10]aneN <sub>2</sub> S	
		[32]	[12]	[33]	[28]	[32]	[12]	[33]	[33]
Metal cation									
Co(II)	$\log K_1$	7.85		8.06	5.09			2.97	7.30
	$\log K_2$			7.34		2.76			
Ni(II)	$\log K_1$	10.82	10.45	11.09	7.38	3.44	3.07	3.71	10.10
	$\log K_2$	9.95	9.60	10.01	6.14	3.81	3.46	3.87	
Cu(II)	$\log K_1$		12.42	12.66	9.02		3.40	3.64	11.59
	$\log K_2$		9.87	10.25	5.24		4.63	5.01	
Zn(II)	$\log K_1$	7.31		7.54	5.31	2.00		2.23	6.85
	$\log K_2$	5.84		6.06	3.57	2.27		2.49	
Cd(II)	$\log K_1$	6.65		6.82	5.47	1.18		1.35	6.50
	$\log K_2$	5.81		5.95	3.52	2.29		2.43	11.20
Pb(II)	$\log K_1$	6.76		6.90		6.0	0.76	0.90	

<sup>a</sup> $\log K_{(\text{mac})}$  is the magnitude of the macrocyclic effect, i.e.  $\log K$  for the macrocyclic complex minus  $\log K$  for the open chain analogue complex.

Interestingly, there is a tendency for  $\log K_{(\text{mac})}$  to decrease for complexes of [9]aneN<sub>2</sub>S as the ionic radius of the metal increases (Table 2). This is in agreement with the molecular mechanics calculations which suggest that ligands of the type [9]aneX<sub>3</sub> (X=N,O,S,) co-ordinate to the smaller metal cations with the lowest strain energy [33,34].

#### 4. Metal complexes of [9]aneN<sub>2</sub>S, [10]aneN<sub>2</sub>S, [9]aneNS<sub>2</sub> and [10]aneNS<sub>2</sub>

Considering [9]aneN<sub>2</sub>S was first synthesised in 1982, relatively little co-ordination chemistry of this ligand has been reported, and this applies more so to [10]aneN<sub>2</sub>S, [9]aneNS<sub>2</sub> and [10]aneNS<sub>2</sub>. This probably reflects the greater difficulty in preparing these mixed-donor ligands, when compared to the relative ease of preparation of [9]aneN<sub>3</sub> and [9]aneS<sub>3</sub>. The following section reviews the co-ordination studies that have thus far been published with these mixed-donor systems.

##### 4.1. Vanadium

The reaction of VCl<sub>3</sub> with [9]aneN<sub>2</sub>S affords the V(IV) compound [VOCl<sub>2</sub>([9]aneN<sub>2</sub>S)]MeCN [35], oxidation of V(III) to V(IV) occurring presumably by traces of O<sub>2</sub> present in the crystallisation process. The crystal structure reveals the macrocycle facially capping the metal centre, V–S=2.689(1), V–N=2.153(1), 2.150(1) Å. The  $\pi$ -donor oxo group is *trans* to the S-donor of the macrocycle, V–O=1.632(2) Å and exerts a marked *trans* effect upon the V–S bond of 2.689(1) Å. The co-ordination sphere is completed by two Cl<sup>–</sup> ions, V–Cl = 2.337(1), 2.346(1) Å.

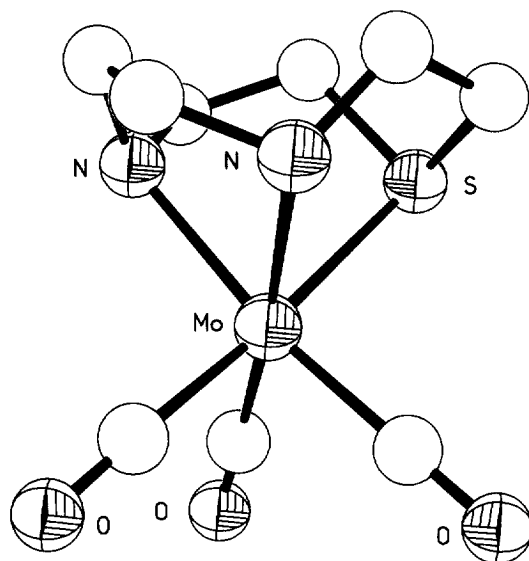
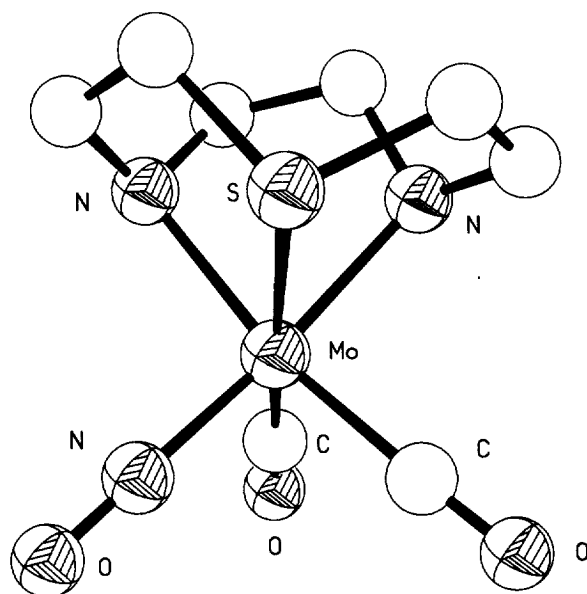
##### 4.2. Molybdenum and tungsten

The reaction of Mo(CO)<sub>6</sub> and W(CO)<sub>6</sub> with [9]aneN<sub>2</sub>S affords the complexes [Mo([9]aneN<sub>2</sub>S)(CO)<sub>3</sub>] and [W([9]aneN<sub>2</sub>S)(CO)<sub>3</sub>] in very good yields [14]. The crystal structure of [Mo([9]aneN<sub>2</sub>S)(CO)<sub>3</sub>] (Fig. 3) shows the metal in a distorted octahedral geometry, Mo–N=2.317(6), and 2.292(5), Mo–S = 2.526(2), Mo–Cl = 1.924(6), 1.926(6), and 1.952(6) Å.

The reaction of [M([9]aneN<sub>2</sub>S)(CO)<sub>3</sub>] (M=Mo, W) with an aqueous solution of NaNO<sub>2</sub> followed by treatment with acid gives the nitrosyl derivative [M([9]aneN<sub>2</sub>S)(CO)<sub>2</sub>(NO)]PF<sub>6</sub>, while prolonged exposure to NaNO<sub>2</sub>/HCl affords the fully decarbonylated green nitrosyl complexes [MCl([9]aneN<sub>2</sub>S)(NO)<sub>2</sub>](X), (X=ClO<sub>4</sub><sup>–</sup> or PF<sub>6</sub><sup>–</sup>) [36].

The structure of [Mo([9]aneN<sub>2</sub>S)(CO)<sub>2</sub>(NO)]PF<sub>6</sub> (Fig. 4) shows the Mo centre in a distorted octahedral geometry with the macrocycle co-ordinating facially, Mo–N=2.244(2), 2.256(2) and Mo–S=2.522(1) Å. The strong  $\pi$ -acceptor NO<sup>+</sup> ligand is co-ordinated *trans* to a N-donor of the macrocycle, Mo–N=1.874(3) Å.



Fig. 3. Structure of  $[\text{Mo}([\text{9}] \text{aneN}_2\text{S})(\text{CO})_3]$ .Fig. 4. Structure of  $[\text{Mo}([\text{9}] \text{aneN}_2\text{S})(\text{CO})_2(\text{NO})]^+$ .

The co-ordination sphere is completed by two CO ligands, Mo–C=1.942(1) and 2.013(3) Å. In the structure of  $[\text{Mo}([\text{9}] \text{aneN}_2\text{S})(\text{NO})_2\text{Cl}]\text{PF}_6$  (Fig. 5) the macrocycle binds facially to the metal centre, Mo–N=2.222(7) and 2.234(6) and Mo–S=

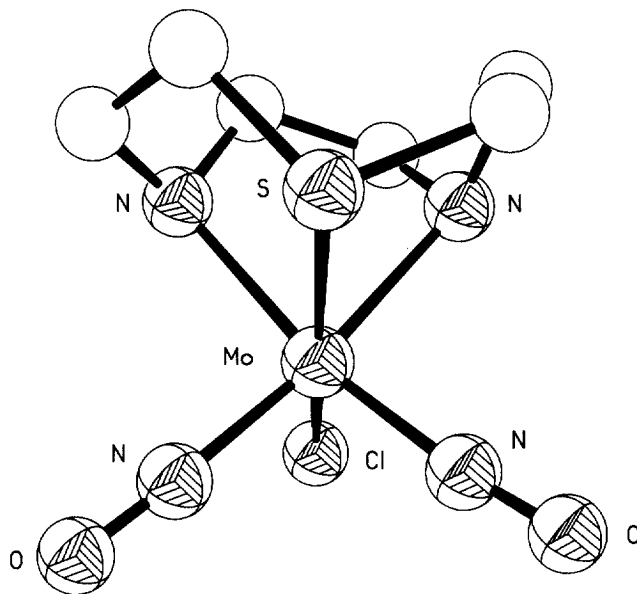


Fig. 5. Structure of  $[\text{Mo}([9]\text{aneN}_2\text{S})(\text{NO})_2\text{Cl}]^+$

2.447(2) Å. The two NO ligands are *trans* to the N-donors of the macrocycle  $\text{Mo}-\text{N}=1.819(7)$ ,  $1.824(7)$  Å, and the  $\text{Cl}^-$  ligand is *trans* to the sulfur atom of the macrocycle,  $\text{Mo}-\text{Cl}=2.440(2)$  Å.

$[\text{Mo}([9]\text{aneN}_2\text{S})(\text{CO})_3]$  undergoes similar oxidative-addition reactions to  $[\text{Mo}([9]\text{aneN}_3)(\text{CO})_3]$  [37–40] with halogens to give seven co-ordinate divalent complexes of the type  $[\text{Mo}([9]\text{aneN}_2\text{S})(\text{CO})_3\text{X}]\text{X}$  ( $\text{X}=\text{Cl}^-$ ,  $\text{Br}^-$ ,  $\text{I}^-$ ) [35]. Metathesis with  $\text{PF}_6^-$  in EtOH affords the complexes  $[\text{Mo}([9]\text{aneN}_2\text{S})(\text{CO})_3\text{X}]^+$  ( $\text{X}=\text{Cl}^-$ ,  $\text{Br}^-$ ) as stable  $\text{PF}_6^-$  salts [35]. Prolonged exposure of  $[\text{Mo}([9]\text{aneN}_2\text{S})(\text{CO})_3]$  to  $\text{Br}_2$  in MeCN affords  $[\text{Mo}([9]\text{aneN}_2\text{S})(\text{O})\text{Br}_2]\text{Br}$ , hydrolysis of which with HCl yields the dimeric cation  $[\text{Mo}_2([9]\text{aneN}_2\text{S})_2(\text{O})_4]^{2+}$  as  $\text{PF}_6^-$  or  $\text{ClO}_4^-$  salts [36]. The  $[\text{ZnCl}_4]^{2-}$  salt of this cation was crystallised and structurally characterised (Fig. 6). The compound consists of the bis( $\mu$ -oxo)bis[oxo( $[9]\text{aneN}_2\text{S})\text{Mo}(\text{V})$ ] cation with the  $\text{Mo}=\text{O}$  groups in mutually *syn* positions,  $\text{Mo}(1)-\text{O}(1)=1.939(5)$ ,  $\text{Mo}(1)-\text{O}2=1.934(5)$ ,  $\text{Mo}(1)-\text{O}(3)=1.674(5)$ ,  $\text{Mo}(1)-\text{N}(1)=2.316(5)$ ,  $\text{Mo}(1)-\text{N}(2)=2.237(5)$ ,  $\text{Mo}(1)-\text{S}(1)=2.716(2)$ ,  $\text{Mo}(1)-\text{Mo}(2)=2.549(1)$  Å.

Treatment of solutions of  $[\text{Mo}_2([9]\text{aneN}_2\text{S}_2(\text{O})_4)(\text{ClO}_4)_2]$  with HCl leads to a colour change from orange to green and the reaction is reversed upon basification with NaOH. The green species was shown to be  $[\text{Mo}_2([9]\text{aneN}_2\text{S}_2(\text{O})_3\text{Cl}_2)(\text{ClO}_4)_2]$  and although no crystallographic evidence was presented, IR spectroscopy confirmed the presence of  $\nu_{\text{Mo}=\text{O}}$  and  $\nu_{\text{Mo}-\text{O}-\text{Mo}}$  stretching vibrations indicative of a  $\text{Mo}_2\text{O}_3$  core [35].

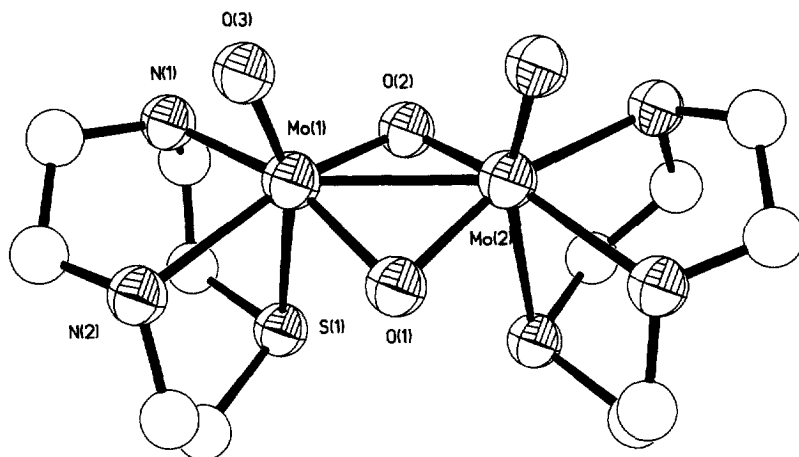


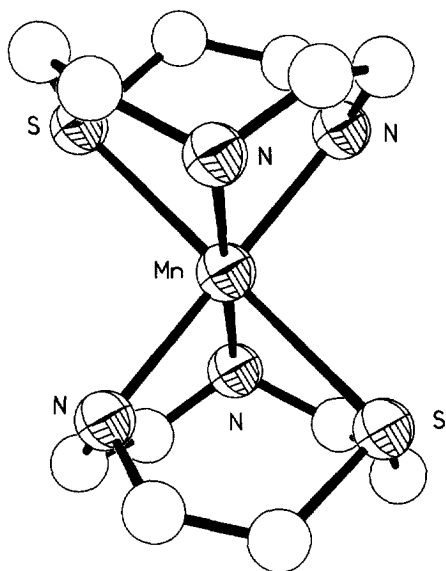
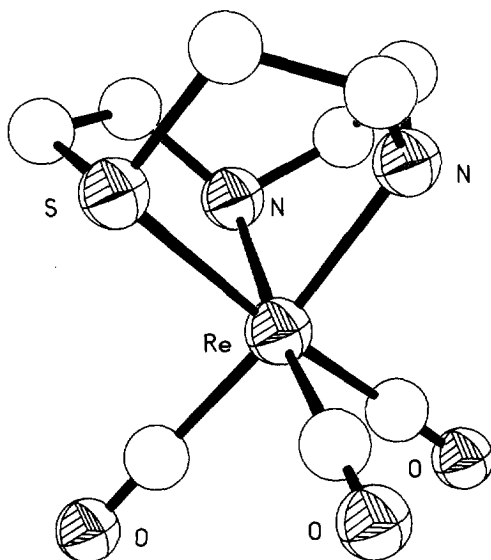
Fig. 6. Structure of  $[\text{Mo}_2(\text{[9]aneN}_2\text{S})_2(\text{O})_4]^{2+}$ .

Reaction of  $[\text{Mo}(\text{[9]aneN}_2\text{S})(\text{CO})_3]$  with  $\text{HCl}$  in the presence of air affords  $[\text{Mo}(\text{[9]aneN}_2\text{S})\text{Cl}_3]$  [36], the crystal structure of which shows the  $\text{Mo}(\text{III})$  centre to be in a distorted octahedral geometry,  $\text{Mo}-\text{N}=2.193(3)$  and  $2.209(4)$ ,  $\text{Mo}-\text{S}=2.467(1)$ ,  $\text{Mo}-\text{Cl}=2.425(1)$ ,  $2.408(1)$  and  $2.426(1)$  Å. Reaction of  $[\text{Mo}(\text{[9]aneN}_2\text{S})(\text{CO})_3]$  with  $\text{HNO}_3$  leads to oxidation of the ligand even in dilute solutions, the IR spectrum showing a strong peak at  $1150\text{ cm}^{-1}$  indicative of a  $\text{S}=\text{O}$  stretching vibration [36].

#### 4.3. Manganese and rhenium

Hanson and co-worker have reported [41] the structure of  $[\text{Mn}(\text{[9]aneN}_2\text{S})_2(\text{ClO}_4)_2]$  (Fig. 7) which shows the  $\text{Mn}(\text{II})$  cation bound to all six donors of the two crowns resulting in a distorted octahedral geometry for the complex. The bond lengths for the centrosymmetric cation,  $\text{Mn}-\text{S}=2.625(3)$ ,  $\text{Mn}-\text{N}=2.242(7)$  Å, show four short interactions to the N-donors and two longer interactions to the S-donors. The N-donors occupy the equatorial plane and the thioether donors the axial sites. The magnetic moment for the complex at 298 K is  $5.82\text{ }\mu_{\text{B}}$ , which is slightly lower than the spin only value of  $5.92\text{ }\mu_{\text{B}}$  and is indicative of a high spin ( $S=5/2$ ) configuration. [42] The effective moment at 4.2 K is lowered to  $5.62\text{ }\mu_{\text{B}}$ , and this is assigned to second-order spin-orbit coupling and the lowering of the symmetry from octahedral, which gives rise to zero-field splitting of the  ${}^6A_{1g}$  state. ESR studies of the complex are in agreement with the  $S=5/2$  spin state indicated by the magnetochemistry.

The reaction of  $\text{Re}(\text{CO})_6\text{Br}$  with  $[\text{9]aneN}_2\text{S}$  affords the complex  $[\text{Re}(\text{[9]aneN}_2\text{S})(\text{CO})_3]\text{Br}$  in very good yield (Fig. 8) [14],  $\text{Re}-\text{N}=2.209(6)$ ,  $2.196(6)$ ,  $\text{Re}-\text{S}=2.441(2)$ ,  $\text{Re}-\text{C}=1.900(7)$ ,  $1.927(7)$ ,  $1.912(7)$  Å.

Fig. 7. Structure of  $[\text{Mn}([9]\text{aneN}_2\text{S})_2]^{2+}$ .Fig. 8. Structure of  $[\text{Re}([9]\text{aneN}_2\text{S})(\text{CO})_3]^+$ .

#### 4.4. Iron and ruthenium

Reaction of  $\text{Fe}(\text{ClO}_4)_2$  with  $[9]\text{aneN}_2\text{S}$  under an inert atmosphere gives the Fe(II) complex  $[\text{Fe}([9]\text{aneN}_2\text{S})_2](\text{ClO}_4)_2$  [35]. The crystal structure of this complex shows

the metal centre in a distorted octahedral geometry, being bound to four nitrogen atoms in a square planar arrangement, Fe–N = 2.072(7), 2.063(6) Å, with two sulfur atoms in the axial positions, Fe–S = 2.337(2) Å. [Fe([9]aneN<sub>2</sub>S)Br]Br<sub>2</sub> can be synthesised by the slow crystallisation of [Fe([9]aneN<sub>2</sub>S)<sub>2</sub>]Br<sub>2</sub> in air. Although no crystallographic data are available, the authors assigned the complex as having a tetrahedral geometry, bound by the macrocycle donors and a Br<sup>−</sup> ligand [35].

Gahan and co-workers have prepared [43] the Fe(III) complex [Fe([9]aneN<sub>2</sub>S)Cl<sub>3</sub>] by reaction of [9]aneN<sub>2</sub>S with hydrated iron(III) chloride. The crystal structure confirms that the metal cation is co-ordinated to the macrocycle and three Cl<sup>−</sup> ions in an overall distorted octahedral geometry, Fe–N = 2.195(1), 2.199(2), Fe–S = 2.549(0), Fe–Cl = 2.331(0), 2.279(0), 2.298(0) Å. The reaction of [Fe([9]aneN<sub>2</sub>S)Cl<sub>3</sub>] with NaOAc, followed by anion metathesis, gives the binuclear complex [Fe<sub>2</sub>O(O<sub>2</sub>CMe)<sub>2</sub>([9]aneN<sub>2</sub>S)<sub>2</sub>](PF<sub>6</sub>)<sub>2</sub> which has two [Fe([9]aneN<sub>2</sub>S)]<sup>3+</sup> moieties linked by two acetate and one oxo ligand. The structure of [Fe<sub>2</sub>O(O<sub>2</sub>CMe)<sub>2</sub>([9]aneN<sub>2</sub>S)<sub>2</sub>](PF<sub>6</sub>)<sub>2</sub> reveals the thioether units to be *trans* to the bridging oxo unit with S–Fe–O bond angles of 175.5(2) and 178.2(2)<sup>o</sup> in a *syn* configuration with respect to the Fe–O–Fe plane [43]. The Fe–S and Fe–N bond lengths in the dimeric complex are similar to those observed in [Fe([9]aneN<sub>2</sub>S)Cl<sub>3</sub>] [43], although lengthening of the Fe–S bond *trans* to the  $\mu$ -oxo ligand is observed from 2.549(0) Å to an average length of 2.573(4) Å for the dimer. This lengthening is due to the *trans* effect of the oxo group. The Mössbauer spectrum of [Fe<sub>2</sub>O(O<sub>2</sub>CMe)<sub>2</sub>([9]aneN<sub>2</sub>S)<sub>2</sub>](PF<sub>6</sub>)<sub>2</sub> confirms the Fe(III) centres to be in the high-spin configuration, and magnetic measurements indicate the Fe(III) centres to be antiferromagnetically coupled,  $J = -125 \text{ cm}^{-1}$  [43].

The half-sandwich complex [Ru([9]aneN<sub>2</sub>S)(cym)][BPh<sub>4</sub>]Cl<sub>2</sub> · MeCN (cym = *p*-Cymene) has been prepared by the reaction of [Ru(cym)Cl<sub>2</sub>]<sub>2</sub> with [9]aneN<sub>2</sub>S [35]. The structure shows the Ru(III) centre bound to the *p*-cymene moiety as well as to the three donors of the macrocycle, Ru–N = 2.120(7), 2.105(7), Ru–S = 2.324(2) Å.

#### 4.5. Cobalt and rhodium

Theoretically, two geometric isomers can exist for complexes of the type [M([9]aneN<sub>2</sub>S)<sub>2</sub>]<sup>n+</sup> and these can be designated *cis* (*syn*) or *trans* (*anti*) according to the arrangement of the sulfur atom around the metal cation. Preparation of the Co(III) complex [Co([9]aneN<sub>2</sub>S)<sub>2</sub>]<sup>3+</sup> was first reported in 1982 [10], with the presence of both *cis* and *trans* isomers recognised by <sup>13</sup>C NMR spectroscopy, although the isomers were not separated. The structure of the *trans* isomer [Co([9]aneN<sub>2</sub>S)<sub>2</sub>](ClO<sub>4</sub>)<sub>3</sub> was first published in 1986 [44]. The complex has a distorted octahedral geometry with the two sulfur atoms *trans* to one another, disorder within the structure giving chelate rings with both conformations in equal probabilities, Co–S = 2.238(1) and Co–N = 1.984(3) Å. The two conformational isomers were separated by Searle and co-workers using fractional crystallisation [45], aided by cation exchange chromatography on SP-sephadex. It was noted that the isomers undergo a base-catalysed isomerisation leading to a *cis/trans* (4:1) equilibrium mix-

ture, with the two isomers readily distinguished by their  $^{13}\text{C}$  NMR spectra. The *cis* isomer has molecular  $\text{C}_2$  symmetry and therefore shows six resonances in the  $^{13}\text{C}$  NMR spectrum. The *trans* isomer, however, has an additional centre of inversion to give a molecular symmetry of  $\text{C}_{2h}$  and therefore only three resonances are observed in the  $^{13}\text{C}$  NMR spectrum [45].

The crystal structure of the *cis*- $[\text{Co}(\text{[9]aneN}_2\text{S})_2]^{3+}$  along with an improved structure of the *trans* isomer has also been reported [46]. The *trans* isomer, *trans*- $[\text{Co}(\text{[9]aneN}_2\text{S})_2]^{3+}$  (Fig. 9) was crystallised as its triflate salt and has an octahedral geometry with two facially co-ordinated ligands,  $\text{Co-S}(1)=2.251(1)$ ,  $\text{Co-S}(2)=2.246(1)$ ,  $\text{Co-N}(1)=1.962(3)$ ,  $\text{Co-N}(2)=1.977(3)$ ,  $\text{Co-N}(3)=1.986(3)$  and  $\text{Co-N}(4)=1.963(3)$  Å. The cation has approximate  $\text{C}_2$  symmetry with the axis passing through the Co centre and bisecting the angles  $\angle\text{N}(1)\text{--Co--N}(4)$  and  $\angle\text{N}(2)\text{--Co--N}(3)$ . The conformation of the five membered chelates is *ldl*, the two rings joined by the sulfur atom having opposite chiralities. This is slightly unusual as all complexes involving the related ligand  $[\text{9]aneN}_3$  have the same chirality (either *ddd* or *lll*).

The *cis* isomer, *cis*- $[\text{Co}(\text{[9]aneN}_2\text{S})_2]^{3+}$  was crystallised as its  $\text{Br}^-$  salt (Fig. 10) [46]. The Co(III) centre has an octahedral field, but with the sulfur atoms mutually *cis* to one another,  $\text{Co-S}=2.217(2)$ ,  $\text{Co-N}=1.979(4)$  and  $1.988(5)$  Å. The Co–N bond lengths are normal but the Co–S bond length is at the short end of the reported range. The shortest previously reported Co–S (thioether) bond length is  $2.226(1)$  Å in  $[\text{Co}(\text{azacpten})]\text{ZnCl}_4\text{Cl}$  (azacpten = 1-methyl-3,13,16-trithia-6,8,10,19-tetraazabicyclo[6,6,6]icosane) [47]. Interestingly, the ligand in *cis*- $[\text{Co}(\text{[9]aneN}_2\text{S})_2]^{3+}$  is in the more usual *lll* conformation with the authors concluding that the *lll* isomer has lower internal strain.

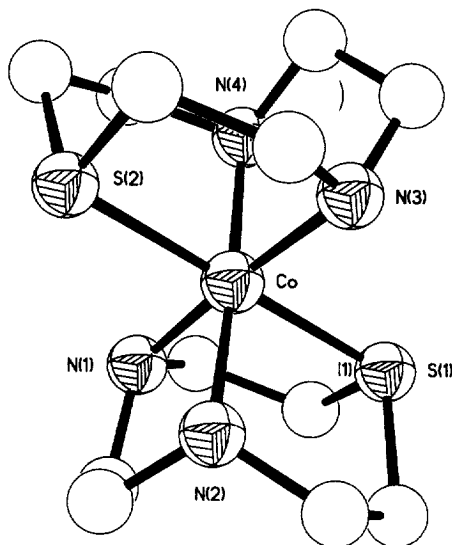


Fig. 9. Structure of *trans*- $[\text{Co}(\text{[9]aneN}_2\text{S})_2]^{3+}$ .

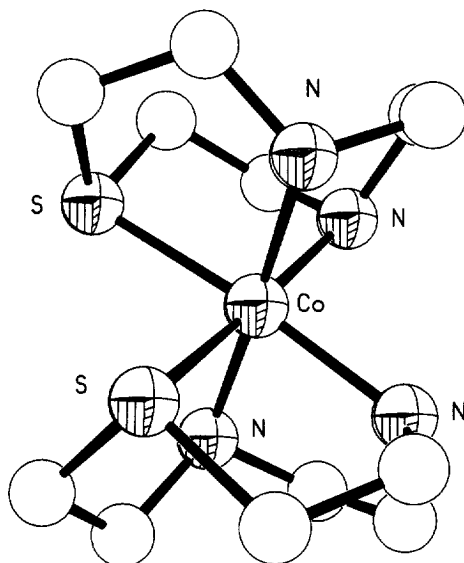
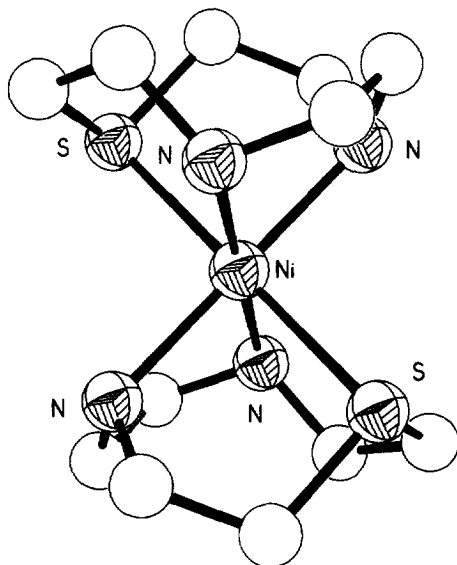
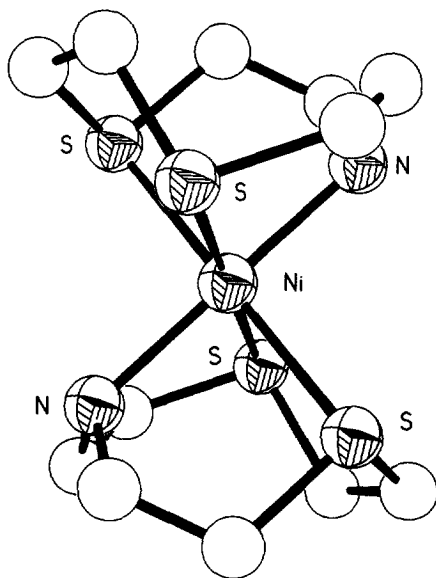


Fig. 10. Structure of *cis*-[Co([9]aneN<sub>2</sub>S)<sub>2</sub>]<sup>3+</sup>.

RhCl<sub>3</sub>·H<sub>2</sub>O reacts with [9]aneN<sub>2</sub>S to give yellow–orange crystals of [Rh([9]aneN<sub>2</sub>S)Cl<sub>3</sub>]·H<sub>2</sub>O [35], which shows the Rh(III) in a distorted octahedral geometry, being bound by the macrocycle as well as three chloride ligands, Rh–N = 2.036(3), 2.040(3), Rh–S = 2.246(1), Rh–Cl = 2.396(1), 2.368(1), 2.358(1) Å.

#### 4.6. Nickel

The crystal structures of [Ni([9]aneN<sub>2</sub>S)<sub>2</sub>]<sup>2+</sup> [12], [Ni([9]aneNS<sub>2</sub>)<sub>2</sub>]<sup>2+</sup> [18], [Ni([10]aneN<sub>2</sub>S)<sub>2</sub>]<sup>2+</sup> [48] and [Ni([10]aneNS<sub>2</sub>)<sub>2</sub>]<sup>2+</sup> [49] have all been determined (Fig. 11 Fig. 12 Fig. 13 Fig. 14, respectively). Tables 3 and 4 give the significant bond lengths and angles of these complexes along with those of the homoleptic congeners, [Ni([9]aneN<sub>3</sub>)<sub>2</sub>]<sup>2+</sup> [50], [Ni([9]aneS<sub>3</sub>)<sub>2</sub>]<sup>2+</sup> [51], [Ni([10]aneN<sub>3</sub>)<sub>2</sub>]<sup>2+</sup> [52] and [Ni([10]aneS<sub>3</sub>)<sub>2</sub>]<sup>2+</sup> [53]. The cation [Ni([9]aneN<sub>2</sub>S)<sub>2</sub>]<sup>2+</sup> (Fig. 11) has a centre of symmetry with the two sulfur atoms *trans* to one another, contrasting with the cation [Ni(daes)<sub>2</sub>]<sup>2+</sup> [54] in which the two sulfur atoms are in mutually *cis* positions. The average Ni–N bond lengths for [Ni([9]aneN<sub>2</sub>S)<sub>2</sub>]<sup>2+</sup> and [Ni(daes)<sub>2</sub>]<sup>2+</sup> are similar, indicating no compression of bond lengths of the macrocycle relative to the acyclic congener. The Ni–N distances are also very close to the strain-free bond length of 2.10 Å [55]. The Ni–S bond length of [Ni([9]aneN<sub>2</sub>S)<sub>2</sub>]<sup>2+</sup> is slightly shorter than that of [Ni(daes)<sub>2</sub>]<sup>2+</sup> reflecting the steric effects of a more constrained macrocyclic system. The structure of [Ni([9]aneNS<sub>2</sub>)<sub>2</sub>]<sup>2+</sup> (Fig. 13) shows octahedral co-ordination at the metal centre with the two nitrogen atoms *trans* to one another and the four S-donors and the Ni(II) centre lying in the equatorial plane. The Ni–N bond length is very similar to that in [Ni([9]aneN<sub>3</sub>)<sub>2</sub>]<sup>2+</sup> [50], and only slightly

Fig. 11. Structure of [Ni([9]aneN<sub>2</sub>S<sub>2</sub>)<sub>2</sub>]<sup>2+</sup>.Fig. 12. Structure of [Ni([9]aneNS<sub>2</sub>)<sub>2</sub>]<sup>2+</sup>.

shorter than in [Ni([9]aneN<sub>2</sub>S)<sub>2</sub>]<sup>2+</sup> [12]. The Ni–S distances are also very similar to those in [Ni([9]aneN<sub>2</sub>S)<sub>2</sub>]<sup>2+</sup> but are appreciably longer than those in [Ni([9]aneS<sub>3</sub>)<sub>2</sub>]<sup>2+</sup>. Complexes of the 10-membered ring macrocycles all show a slight



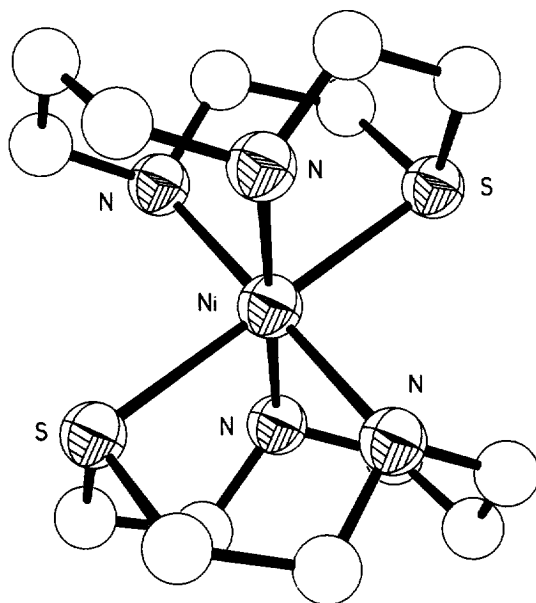


Fig. 13. Structure of  $[\text{Ni}([\text{10}] \text{aneN}_2\text{S})_2]^{2+}$ .

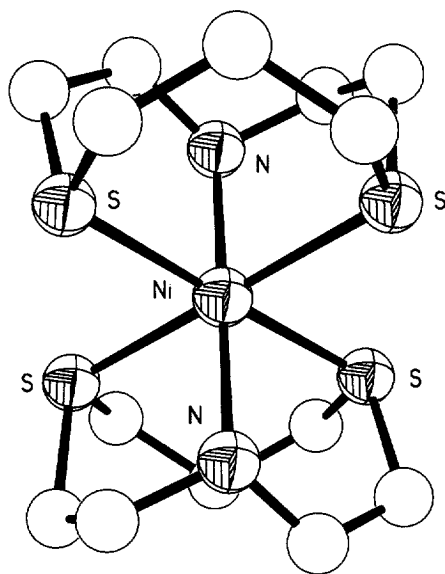


Fig. 14. Structure of  $[\text{Ni}([\text{10}] \text{aneNS}_2)_2]^{2+}$ .

Table 3

Significant bond lengths of the Ni(II) complexes of tridentate macrocycles

Complex	Bond lengths (Å)		Refs
	Ni–N	Ni–S	
[Ni([9]aneN <sub>3</sub> ) <sub>2</sub> ] <sup>2+</sup>	2.102(4) 2.098(4) 2.111(4)		[50]
[Ni([9]aneN <sub>2</sub> S) <sub>2</sub> ] <sup>2+</sup>	2.11(2) 2.108(2)	2.418(1)	[12]
[Ni([9]aneNS <sub>2</sub> ) <sub>2</sub> ] <sup>2+</sup>	2.104(4)	2.408(1) 2.415(1)	[18]
[Ni([9]aneS <sub>3</sub> ) <sub>2</sub> ] <sup>2+</sup>		2.377(1) 2.380(1) 2.400(1)	[51]
[Ni(daes) <sub>2</sub> ] <sup>2+</sup>	2.11(1)	2.455(5) 2.463(6)	[54]
[Ni([10]aneN <sub>3</sub> ) <sub>2</sub> ] <sup>2+</sup>	2.124(4) 2.102(4) 2.143(4)		[52]
[Ni([10]aneN <sub>2</sub> S) <sub>2</sub> ] <sup>2+</sup>	2.141(5) 2.143(4)	2.395(1)	[48]
[Ni([10]aneNS <sub>2</sub> ) <sub>2</sub> ] <sup>2+</sup>	2.125(5)	2.408(2) 2.407(2)	[49]
[Ni([10]aneS <sub>3</sub> ) <sub>2</sub> ] <sup>2+</sup>		2.403(2) 2.386(2) 2.396(2)	[53]

Table 4

Significant bond angles for the Ni(II) complexes of tridentate macrocycles

Complex	Bond angles			Refs
	N–Ni–N	S–Ni–N	S–Ni–S	
[Ni([9]aneN <sub>3</sub> ) <sub>2</sub> ] <sup>2+</sup>	82.5			[50]
[Ni([9]aneN <sub>2</sub> S) <sub>2</sub> ] <sup>2+</sup>	80.5	85.1		[12]
[Ni([9]aneNS <sub>2</sub> ) <sub>2</sub> ] <sup>2+</sup>		85.0	87.4	[18]
[Ni([9]aneS <sub>3</sub> ) <sub>2</sub> ] <sup>2+</sup>			88.0	[51]
[Ni([10]aneN <sub>3</sub> ) <sub>2</sub> ] <sup>2+</sup>	82.4			[52]
[Ni([10]aneN <sub>2</sub> S) <sub>2</sub> ] <sup>2+</sup>	87.1	85.5		[48]
[Ni([10]aneNS <sub>2</sub> ) <sub>2</sub> ] <sup>2+</sup>		85.4	95.8*	[49]
[Ni([10]aneS <sub>3</sub> ) <sub>2</sub> ] <sup>2+</sup>			89.2, 94.1*	[53]

\*Six membered chelate ring.

lengthening of the Ni–N bond length and concomitant shortening of the Ni–S bond distance compared to their nine-membered ring derivatives. In both the nine- and 10-membered ring complexes, the bite angle for the five-membered chelate ring increases towards the ideal octahedral angle of 90° as N-donors are replaced by S-donors (Table 4).

Table 5

Electronic spectra for the Ni(II) complexes of tridentate macrocycles

Complex	$\lambda_{\text{max}}$ , nm ( $\epsilon$ , $\text{M}^{-1} \text{cm}^{-1}$ )				10 Dq, $\text{cm}^{-1}$	B, $\text{cm}^{-1}$	Refs
[Ni([9]aneN <sub>3</sub> ) <sub>2</sub> ] <sup>2+</sup>	870	800(7)	505(5)	308(12)	12500	993	[50]
[Ni([9]aneN <sub>3</sub> S) <sub>2</sub> ] <sup>2+</sup>	930	854	548	350	11770	820	[12]
[Ni([9]aneNS <sub>2</sub> ) <sub>2</sub> ] <sup>2+</sup>	840(22.5)		524(15)	297(680)	11904		[18]
[Ni([9]aneS <sub>3</sub> ) <sub>2</sub> ] <sup>2+</sup>	784(27)		527(26)	325	12760	680	[51]
[Ni([10]aneN <sub>3</sub> ) <sub>2</sub> ] <sup>2+</sup>	870	800	513	327	12500	937	[52]
[Ni([10]aneN <sub>2</sub> S) <sub>2</sub> ] <sup>2+</sup>	960	863(14)	529(14)	350	11588	880	[48]
[Ni([10]aneNS <sub>2</sub> ) <sub>2</sub> ] <sup>2+</sup>	843(10)		526(14)	418(25)	11844	778	[49]
[Ni([10]aneS <sub>3</sub> ) <sub>2</sub> ] <sup>2+</sup>	850	800(37)	530(66)		12500	717	[53]

The electronic spectra for the Ni(II) complexes are summarised in Table 5. Difficulties arise when trying to gain accurate ligand-field parameters for the mixed-donor complexes, partly due to the fact that the spin forbidden  $^3A_{2g} - ^1E_g$  transition is observed very close to the transition from which the 10 Dq value is calculated  $^3A_{2g} - ^3E_g$ . An equation modified by Hancock [12] for the complexes where N and S are donors has been proposed to give more representative values of 10 Dq. From Table 5 it can be seen that in the case of the 9- and 10- membered ring systems the 10 Dq values are the highest when the ligand systems are homoleptic i.e. all N- or all S-donors. When mixed S/N donor sets are introduced however the 10 Dq value decreases. This is due to the fact that ring-strain is at a minimum when all the donors are the same, whereas mixed-donor systems lead to higher ring-strain and therefore lower 10 Dq values. From Table 5 it can also be seen that the Racah parameter B decreases as the harder nitrogen atoms are gradually replaced by the softer sulfur atoms. Increasing the number of S atoms in the donor set allows greater delocalisation of the  $t_{2g}$  electron density into the low-lying ligand orbitals. This in turn reduces inter-electron repulsions and therefore the Racah parameter B.

Cyclic voltammetry of [Ni([9]aneNS<sub>2</sub>)<sub>2</sub>]<sup>2+</sup> shows a reversible one-electron process assigned to the Ni(II)/(III) couple at  $E_{1/2} = 1.044\text{V}$  vs NHE. The formation of the Ni(III) species [Ni([9]aneNS<sub>2</sub>)<sub>2</sub>]<sup>3+</sup> was confirmed by ESR spectroscopy [18]. An irreversible reduction wave at  $E_{1/2} = -1.52\text{V}$  was also observed for [Ni([9]aneNS<sub>2</sub>)<sub>2</sub>]<sup>2+</sup>.

The  $E_{1/2}$  values for the Ni(II)/(III) couples for the 10-membered macrocyclic complexes are shown in Table 6 [48,49,52,53]. The redox potentials shift anodically as the harder N-donor atoms are replaced by the softer S-donor atoms. This is consistent with the ability of S-donor ligands to stabilise Ni(II) relative to Ni(III) and for N-donor ligands to accommodate the Ni(III) state more readily.

#### 4.7. Palladium and platinum

An intriguing aspect of the co-ordination chemistry of tridentate ligands to Pd(II) and Pt(II) cations is the inherent mismatch between the preferred geometries of the

Table 6

Redox potentials ( $\text{Ni}^{2+}/^{3+}$ ) for Ni(II) complexes of 10-membered macrocyclic ligands

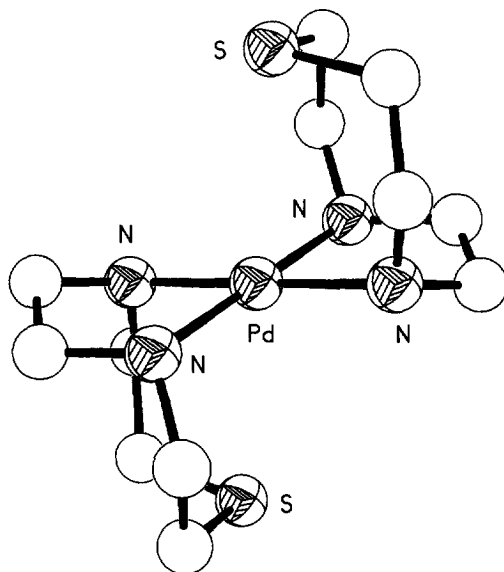
Complex	$E_{1/2}$ (V)	Ref.
$[\text{Ni}([\text{10}] \text{aneN}_3)_2]^{2+}$	0.997 <sup>a</sup>	[52]
$[\text{Ni}([\text{10}] \text{aneN}_2\text{S})_2]^{2+}$	1.21 <sup>a</sup>	[48]
$[\text{Ni}([\text{10}] \text{aneNS}_2)_2]^{2+}$	1.26 <sup>b</sup>	[49]
$[\text{Ni}([\text{10}] \text{aneS}_3)_2]^{2+}$	1.30 <sup>b</sup>	[53]

<sup>a</sup>Aqueous media.<sup>b</sup>MeCN.

metal and the ligand centres. Pd(II) and Pt(II) are both  $d^8$  metal centres and have therefore a very strong preference for square-planar geometry, whereas the tridentate family of ligands have a predisposition for co-ordination to triangular faces of an octahedron.

A number of complexes have been obtained on reaction of Pd(II) salts with [9]aneN<sub>2</sub>S, depending on the counterion and the conditions used for complexation [56,57]. Reaction of Pd(OAc)<sub>2</sub> with [9]aneN<sub>2</sub>S in methanol followed by anion metathesis with NaPF<sub>6</sub> gives the complex  $[\text{Pd}([\text{9}] \text{aneN}_2\text{S})_2](\text{PF}_6)_2$ . [56] The crystal structure of  $[\text{Pd}([\text{9}] \text{aneN}_2\text{S})_2](\text{PF}_6)_2$  consists (Fig. 15) of a square-planar Pd(II) centre bound to the four N-donors of the two macrocycle centres, Pd–N = 2.065(3), 2.054(3) Å, with the thioether S-donors showing long-range apical interactions to the Pd(II) centre, Pd...S = 3.033(1) Å.

When [9]aneN<sub>2</sub>S is treated with PdCl<sub>2</sub> at room temperature and irradiated with

Fig. 15. Structure of the cation in  $[\text{Pd}([\text{9}] \text{aneN}_2\text{S})_2](\text{PF}_6)_2$ .

ultrasound for 5 h, the complex  $[\text{Pd}([9]\text{aneN}_2\text{S})_2]\text{Cl}_2 \cdot \text{H}_2\text{O}$  is isolated [57]. The structure of this complex shows (Fig. 16) the Pd(II) cation co-ordinated to four N-donors of the two macrocycles in a square-planar arrangement,  $\text{Pd}-\text{N}=2.047(4)$ ,  $2.058(3)$  Å. However, in contrast to  $[\text{Pd}([9]\text{aneN}_2\text{S})_2](\text{PF}_6)_2$ , the remaining S-donors of the two macrocycles are orientated away from the metal centre and show no interaction. The authors note that in the square-planar complex  $[\text{Pd}([9]\text{aneN}_2\text{S})_2]\text{Cl}_2 \cdot \text{H}_2\text{O}$  the macrocycles are in the [333] conformation, while in the case of  $[\text{Pd}([9]\text{aneN}_2\text{S})_2](\text{PF}_6)_2$  the macrocycles are in the [234] conformation. The cation  $[\text{Pd}([9]\text{aneN}_2\text{S})_2]^{2+}$  has been reported to show fluxional behaviour in solution [58] and this is thought to involve the facile interconversion of the [234] and [333] conformer with the observed conformations in the solid state dictated by the electrostatic forces originating from the different counterions,  $\text{Cl}^-$  and  $\text{PF}_6^-$ .

Reaction of [9]aneN<sub>2</sub>S with PdCl<sub>2</sub> under reflux for several hours gives the complex  $[\text{Pd}([9]\text{aneN}_2\text{S})\text{Cl}_2]$  [57]. Attempts to grow crystals of this complex, however, lead to the isolation of the trinuclear complex  $[\text{Pd}_3([9]\text{aneN}_2\text{S})_4\text{Cl}_2]\text{Cl}_4 \cdot 2\text{H}_2\text{O}$ , the centrosymmetric structure of which (Fig. 17) contains a central  $[\text{Pd}([9]\text{aneN}_2\text{S})_2]^{2+}$  unit with two ligands co-ordinating to the Pd(II) cation *via* the four N-donors,  $\text{Pd}(2)-\text{N}(1)=2.034(9)$ ,  $\text{Pd}(2)-\text{N}(2)=2.070(8)$  Å. The remaining S-donors show weak apical interactions,  $\text{Pd}(2)-\text{S}(1)$  and  $\text{Pd}(2)-\text{S}(1\text{A})=3.008(2)$  Å. S(1) and S(1A) are each co-ordinated to a further  $[\text{Pd}([9]\text{aneN}_2\text{S})\text{Cl}]$  moiety,  $\text{Pd}(1)-\text{N}(3)=2.03(1)$ ,  $\text{Pd}(1)-\text{N}(4)=2.06(1)$ ,  $\text{Pd}(1)-\text{S}(1)=2.308(3)$  and  $\text{Pd}(1)-\text{Cl}(1)=2.308(3)$  Å. The four remaining  $\text{Cl}^-$  centres act as counterions.

The reaction of  $\text{K}_2\text{PtCl}_4$  with [9]aneN<sub>2</sub>S affords, after anion metathesis, the

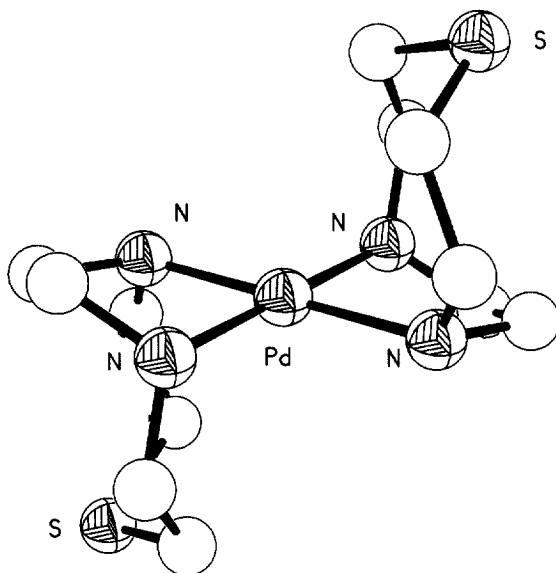
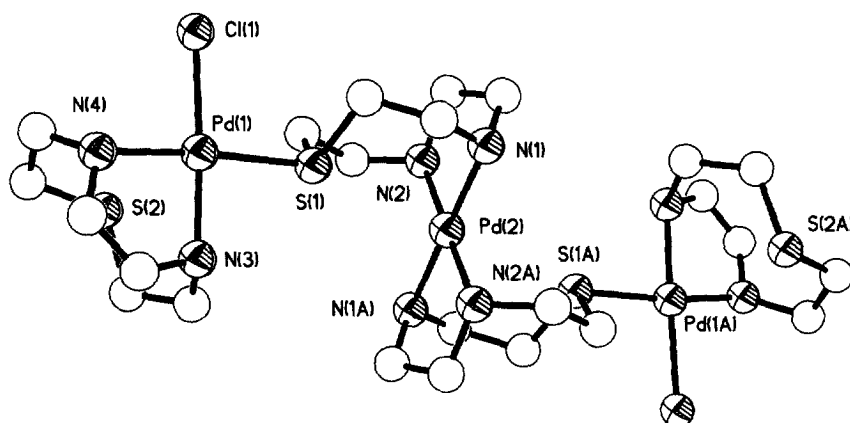
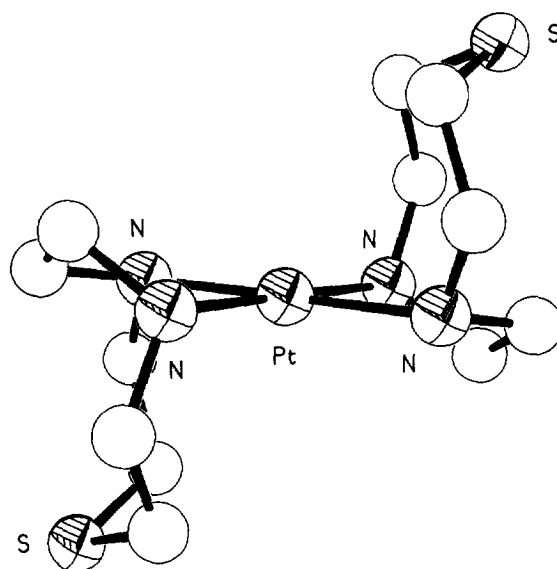
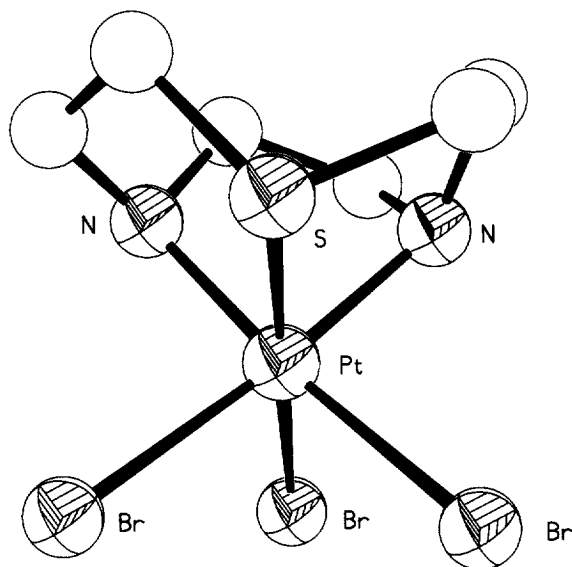


Fig. 16. Structure of the cation in  $[\text{Pd}([9]\text{aneN}_2\text{S})_2]\text{Cl}_2 \cdot \text{H}_2\text{O}$ .

Fig. 17. Structure of  $[\text{Pd}_3([\text{9}] \text{aneN}_2\text{S})_4\text{Cl}_2]^{4+}$ .

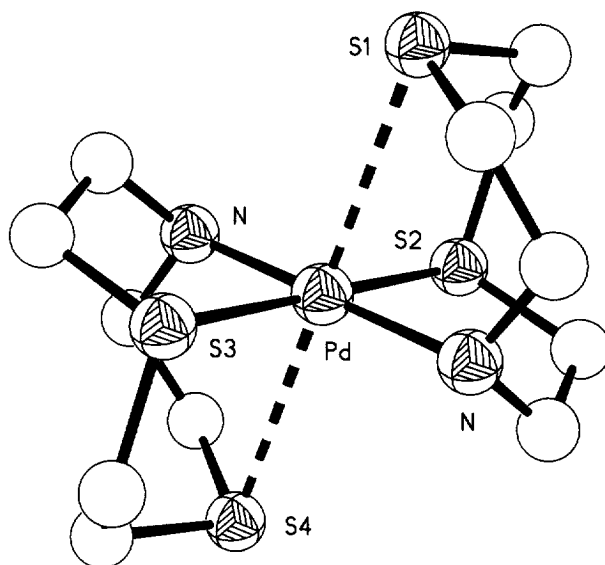
complexes  $[\text{Pt}([\text{9}] \text{aneN}_2\text{S})_2]\text{Br}_2$  [56] and  $[\text{Pt}([\text{9}] \text{aneN}_2\text{S})_2](\text{PF}_6)_2$  [57]. The two compounds are isostructural (Fig. 18) and consist of a Pt(II) cation bound to two  $[\text{9}] \text{aneN}_2\text{S}$  macrocycles in a square-planar geometry *via* four N-donors, Pt–N = 2.08(1) Å [57]. The two remaining sulfur atoms are pointing away from the metal centre and exhibit no interaction to the Pt(II) centre. This is in contrast to  $[\text{Pt}([\text{9}] \text{aneS}_3)_2]^{2+}$ , which shows [59] weak axial co-ordination of the one of the remaining S-donors to the metal centre, Pt–S = 2.885(7) Å.

Fig. 18. Structure of  $[\text{Pt}([\text{9}] \text{aneN}_2\text{S})_2]^{2+}$ .

Fig. 19. Structure of  $[\text{Pt}([9]\text{aneN}_2\text{S})\text{Br}_3]^+$ .

$[\text{Pt}([9]\text{aneN}_2\text{S})_2]^{2+}$  is readily oxidised by atmospheric oxygen to give the Pt(IV) species  $[\text{Pt}([9]\text{aneN}_2\text{S})\text{Br}_3]\text{Br}_{0.5}\text{Cl}_{0.5}$  [60], the structure of which shows (Fig. 19) an octahedral Pt(IV) centre with the macrocycle co-ordinating facially to the metal centre, Pt–N = 2.057(5), 2.038(2), Pt–S = 2.283(3) Å. The remaining co-ordination sphere is made up of three  $\text{Br}^-$  ions, Pt–Br = 2.454(1), 2.457(1), 2.477(1) Å, with the bond angles between all the donor atoms close to 90 or 180°. The counter-anion is a statistically distributed mixture of  $\text{Cl}^-$  or  $\text{Br}^-$  anions over the same crystallographic site. The Pt–Br bond *trans* to the sulfur [2.477(1) Å] is longer than the other two Pt–Br bonds [Pt–Br = 2.454(1), 2.457(1) Å] [60].

$[\text{Pd}([9]\text{aneNS}_2)_2]^{2+}$  has been reported by Schröder and co-workers (Fig. 20) [61], the structure of which is similar to that of  $[\text{Pd}([9]\text{aneN}_2\text{S})_2](\text{PF}_6)_2$  with four short interactions and two long-range contacts. However in the case of  $[\text{Pd}([9]\text{aneNS}_2)_2]^{2+}$ , the Pd(II) centre is co-ordinated to two N- and two S-donors in a square-planar configuration with Pd–N = 2.081(9), Pd–S = 2.322(3) Å. Two long-range apical interactions are provided by the two remaining sulfur atoms, Pd–S = 3.011(3) Å. The electrochemistry of this complex shows two quasi-reversible oxidation waves at  $^1E_{1/2} = 0.43$  V ( $\Delta E_p = 140$  mV) and  $^2E_{1/2} = 0.84$  V ( $\Delta E_p = 130$  mV) vs  $\text{Fc}/\text{Fc}^+$  corresponding to the Pd(II)/Pd(III) and Pd(III)/Pd(IV) redox couples, respectively. Coulometry confirmed that these were two one-electron processes. The ESR spectrum of the electrochemically generated complex  $[\text{Pd}([9]\text{aneNS}_2)_2]^{3+}$  shows a strong signal with  $g_{\parallel} = 2.008$ ,  $g_{\perp} = 2.058$ , typical for a Pd(III) centre [55,56,62–67]. The authors conclude on the basis of previous work, [55,56,65–67] that the lack of hyperfine coupling to the nitrogen is evidence that the N-donors are bound in the equatorial *xy* plane, whilst the S-donors are bound

Fig. 20. Structure of  $[\text{Pd}([\text{9}] \text{aneNS}_2)_2]^{2+}$ .

along the formal  $z$  axis, consistent with the seminal work of Busch and co-workers on Ni(III) complexes of polyaza macrocycles [68,69].

#### 4.8. Copper

The single crystal X-ray structures of the Cu(II) complexes  $[\text{Cu}([\text{9}] \text{aneN}_2\text{S})_2]^{2+}$  [70,71], and  $[\text{Cu}([\text{9}] \text{aneNS}_2)_2]^{2+}$  [21] have been determined and selected bond distances are shown in Table 7, along with the bond distances for the homoleptic analogues,  $[\text{Cu}([\text{9}] \text{aneN}_3)_2]^{2+}$  [72] and  $[\text{Cu}([\text{9}] \text{aneS}_3)_2]^{2+}$  [51]. The structure of

Table 7  
Significant bond lengths for the Cu(II) complexes of tridentate macrocycles

Complex	Bond lengths		Refs
	Cu–N	Cu–S	
$[\text{Cu}([\text{9}] \text{aneN}_3)_2]^{2+}$	2.305(2) 2.048(2) 2.077(2)		[72]
$[\text{Cu}([\text{9}] \text{aneN}_2\text{S})_2]^{2+}$	2.09(1) 2.01(1)	2.707(1)	[70,71]
$[\text{Cu}([\text{9}] \text{aneNS}_2)_2]^{2+}$	2.016(4)	2.547(1) 2.539(1) 2.419(3) 2.426(3) 2.459(3)	[21]
$[\text{Cu}([\text{9}] \text{aneS}_3)_2]^{2+}$			[51]



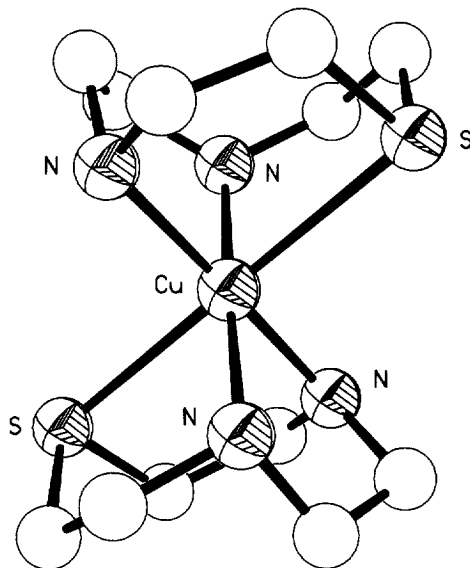
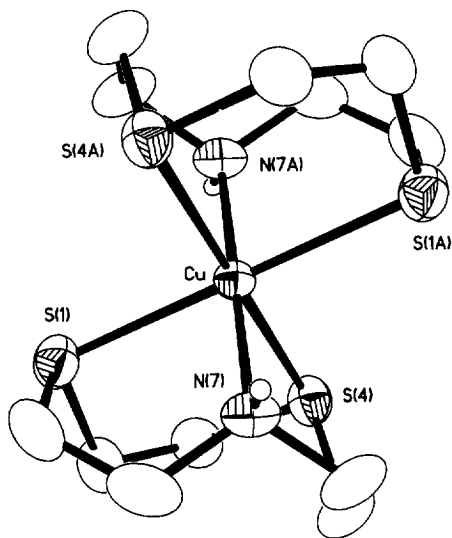
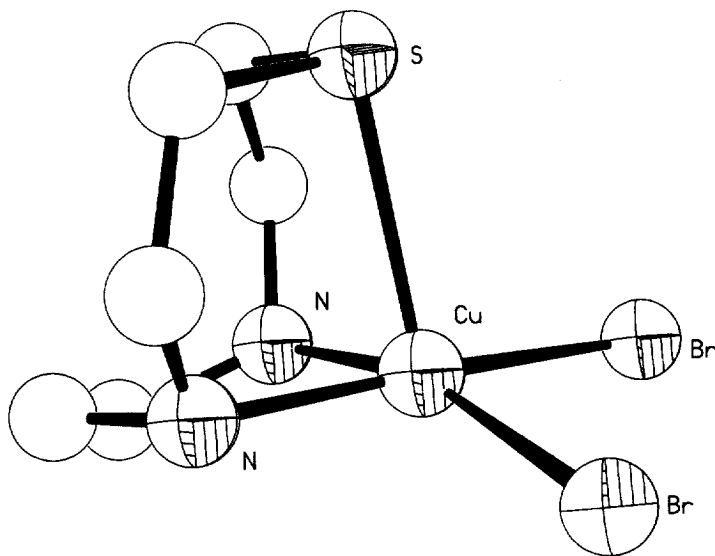


Fig. 21. Structure of  $[\text{Cu}(\text{[9]aneN}_2\text{S})_2]^{2+}$ .

purple  $[\text{Cu}(\text{[9]aneN}_2\text{S})_2]^{2+}$  has been solved, as both  $\text{NO}_3^-$  [70] and  $\text{ClO}_4^-$  [71] salts (Fig. 21). The Cu(II) centre is in a distorted octahedral geometry with four N-donors occupying equatorial sites,  $\text{Cu-N} = 2.027(3), 2.067(3) \text{ \AA}$ . The two sulfur donors occupy axial sites,  $\text{Cu-S} = 2.707(1) \text{ \AA}$  [70], thus giving an overall Jahn–Teller distorted structure. In contrast, the structure of  $[\text{Cu}(\text{[9]aneNS}_2)_2]^{2+}$  shows [21] (Fig. 22) the S-donors occupying the equatorial sites,  $\text{Cu-S} = 2.547(1), 2.539(1) \text{ \AA}$ , and the N-donors at axial positions,  $\text{Cu-N} = 2.016(4) \text{ \AA}$ . Interestingly, single crystal X-ray analysis shows all Cu–S bond lengths in  $[\text{Cu}(\text{[9]aneS}_3)_2]^{2+}$  to be the same [51]. This apparent lack of distortion was assigned to either dynamic Jahn–Teller distortion, or static Jahn–Teller distortion coupled with a positional disorder of cations. For either a time- or space-average structure no distortion would be dent [72].

The reaction of  $\text{CuBr}_2$  with  $[\text{9]aneN}_2\text{S}$  gives green crystals of  $[\text{Cu}(\text{[9]aneN}_2\text{S})\text{Br}_2]$ , the crystal structure of which shows [32] (Fig. 23) a square pyramidal geometry at Cu(II) with a facially co-ordinating  $[\text{9]aneN}_2\text{S}$  ligand,  $\text{Cu-N} = 2.03(1), 2.02(1)$ ,  $\text{Cu-S} = 2.567(3) \text{ \AA}$ . The co-ordination sphere is completed by two  $\text{Br}^-$  ions,  $\text{Cu-Br} = 2.449(2), 2.403(2) \text{ \AA}$ . In the analogous complex  $[\text{Cu}(\text{[9]aneN}_3)\text{Br}_2]$  (Fig. 21) [73] the fifth axial co-ordination site is taken up by the third nitrogen atom of the macrocycle, whereas in  $[\text{Cu}(\text{[9]aneN}_2\text{S})\text{Br}_2]$  this site is taken up by the sulfur atom of the macrocycle.

Although no Cu(I) monomeric complexes of  $[\text{9]aneN}_2\text{S}$  or  $[\text{9]aneNS}_2$  have been isolated, Mattes and co-workers have obtained [74]  $[\text{Cu}_2^{\text{I}}\text{Cu}_2^{\text{II}}(\text{[9]aneN}_2\text{S})_2(\text{CN})_4]\text{SCN}$  by gel diffusion of the sodium salt of [4,7-bis(dithio-

Fig. 22. Structure of  $[\text{Cu}([\text{9}] \text{aneNS}_2)_2]^{2+}$ .Fig. 23. Structure of  $[\text{Pd}([\text{9}] \text{aneN}_2\text{S})\text{Br}_2]$ .

carboxylato) $[\text{9}] \text{aneN}_2\text{S}]^{2-}$  and  $\text{K}_3\text{Cu}(\text{CN})_4$ . The structure of this species consists (Fig. 24) of infinite body of edge-sharing  $[\text{Cu}_2^{\text{I}} \cdot \text{Cu}_2^{\text{II}}]$  tetrahedra with the Cu(I) and Cu(II) centres bridged via  $\text{CN}^-$  bridges.  $[\text{9}] \text{aneN}_2\text{S}$  is co-ordinated facially to Cu(II),  $\text{Cu}-\text{N}=2.042(2)$ ,  $2.035(2)$ ,  $\text{Cu}-\text{S}=2.556(2)$  Å. The two remaining

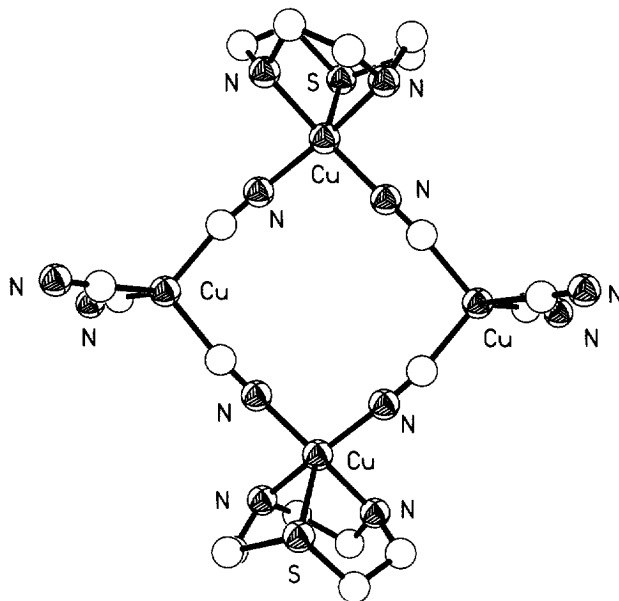


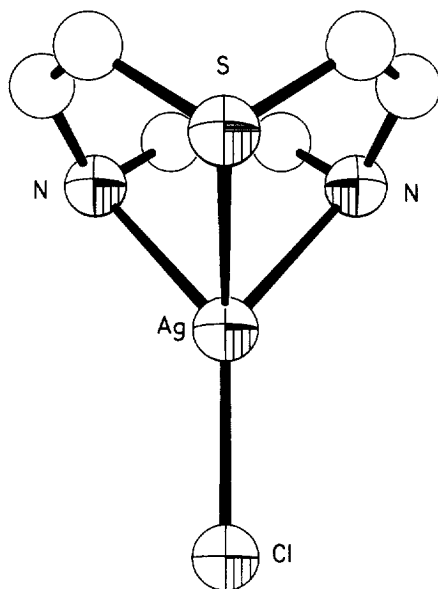
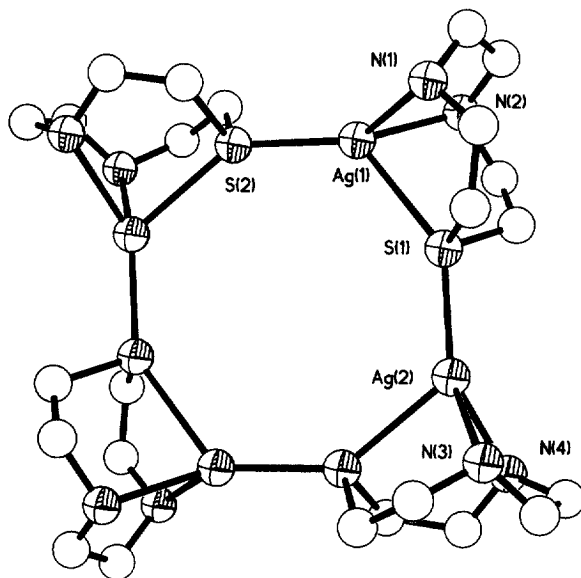
Fig. 24. Structure of  $[\text{Cu}_2^{\text{I}}\text{Cu}_2^{\text{II}}([\text{9}] \text{aneN}_2\text{S})_2(\text{CN})_4]^+$ .

co-ordination sites of Cu are taken by N-bound  $\text{CN}^-$  anions  $\text{Cu}-\text{N}=1.959(2)$ ,  $1.972(3)$  Å. The two nitrogen donors of the macrocycle and two  $\text{CN}^-$  make up the base of the square, and the remaining S-donor of the macrocycle is at an axial site. The Cu(I) centres are four co-ordinate, being bound to four  $\text{CN}^-$  ligands in the preferred tetrahedral geometry.

#### 4.9. Silver and gold

Reaction of  $\text{AgCl}$  with  $[\text{9}] \text{aneN}_2\text{S}$  affords colourless crystals of  $[\text{Ag}([\text{9}] \text{aneN}_2\text{S})\text{Cl}]$  [75], the structure of which shows (Fig. 25) tetrahedral co-ordination at  $\text{Ag}(\text{I})$  with a facially co-ordinated macrocycle,  $\text{Ag}-\text{N}=2.414(5)$ ,  $\text{Ag}-\text{S}=2.629(2)$  Å and one  $\text{Cl}^-$  ligand,  $\text{Ag}-\text{Cl}=2.399(2)$  Å. The structure is comparable to that of  $[\text{Ag}([\text{9}] \text{aneN}_3\text{SCN})]$  [76] which has a mean  $\text{Ag}-\text{N}$  distance of 2.407 Å. In the presence of non-co-ordinating anions such as  $\text{CF}_3\text{SO}_3^-$  and  $\text{ClO}_4^-$  a tetranuclear complex with the stoichiometry,  $[\text{Ag}_4([\text{9}] \text{aneN}_2\text{S})_4]^{4+}$  is isolated [57] (Fig. 26). In this structure  $\text{Ag}(\text{I})$  is four co-ordinate and is facially bound to the macrocycle, with the thioether S-donor bridging to another  $[\text{Ag}([\text{9}] \text{aneN}_2\text{S})]^+$  fragment to give a tetrameric structure,  $\text{Ag}(1)-\text{S}(1)=2.635(2)$ ,  $\text{Ag}(1)-\text{N}(1)=2.332(8)$ ,  $\text{Ag}(1)-\text{N}(2)=2.369(9)$ ,  $\text{Ag}(1)-\text{S}(2)=2.415(2)$  Å.

Two products have been obtained from the reaction of  $\text{Au}(\text{III})$  salts with  $[\text{9}] \text{aneN}_2\text{S}$ , namely  $[\text{Au}([\text{9}] \text{aneN}_2\text{S})\text{Cl}_2](\text{AuCl}_4)$  and  $[\text{Au}([\text{9}] \text{aneN}_2\text{S})\text{Cl}_2]\text{Cl}$  [57].

Fig. 25. Structure of  $[\text{Ag}([9]\text{aneN}_2\text{S})\text{Cl}]$ .Fig. 26. Structure of  $[\text{Ag}_4([9]\text{aneN}_2\text{S})_4]^{4+}$ .

Only the former has been crystallised and structurally characterised (Fig. 27). The Au(III) centre in  $[\text{Au}([9]\text{aneN}_2\text{S})\text{Cl}_2]^+$  is four co-ordinate, being bound in a planar geometry by the two N-donors,  $\text{Au}-\text{N}=2.065(8)$ ,  $2.068(8)$  Å, and two  $\text{Cl}^-$  ions,

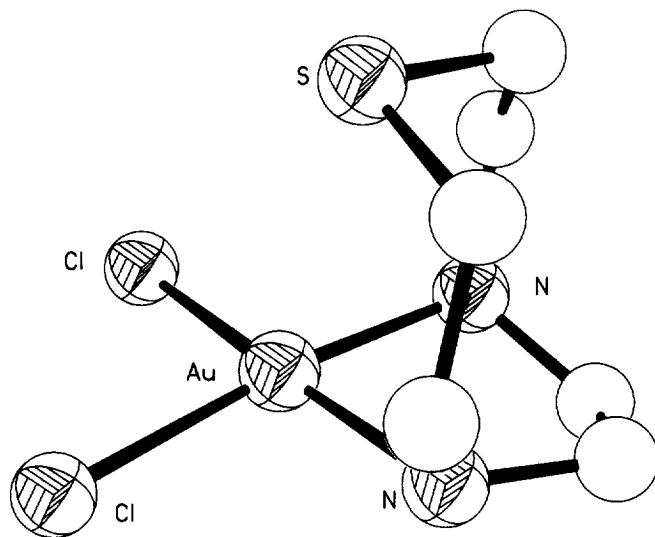


Fig. 27. Structure of the cation in  $[\text{Au}([9]\text{aneN}_2\text{S})\text{Cl}_2](\text{AuCl}_4)$ .

$\text{Ag}-\text{Cl}=2.286(3)$ ,  $2.269(4)$  Å. The S-donor of the macrocycle takes part in an additional long-range apical interaction to the metal centre at a distance of  $2.973(3)$  Å [57].

#### 4.10. Zinc and mercury

$[\text{Zn}([9]\text{aneN}_2\text{S})_2](\text{PF}_6)_2$  and  $[\text{Zn}([9]\text{aneN}_2\text{S})_2][\text{ZnCl}_4]$  have been prepared and structurally characterised [35]. Selected bond lengths are shown in Table 8. In both cations the four N donors of the two macrocycles occupy the equatorial plane and the two S donors are in the axial positions. The Zn–S bond distances are very similar, though the Zn–N bond distances vary slightly between the  $\text{PF}_6^-$  and the  $\text{ZnCl}_4^{2-}$  complexes the average values being 2.144 and 2.170 Å, respectively. The authors conclude that this is due to strong hydrogen bonds between the N–H and the Zn–Cl of the anion.

$[\text{Zn}([9]\text{aneNS}_2)_2]\text{BF}_4$  has been prepared from the reaction of hydrated  $\text{Zn}(\text{BF}_4)_2$  and [9]aneNS<sub>2</sub> and has been structurally characterised (A.J. Amoroso,

Table 8  
Significant bond lengths for the Zn(II) complexes of [9]aneN<sub>2</sub>S

Complex	Bond lengths			Refs
	Zn–S1	Zn–N1	Zn–N2	
$[\text{Zn}([9]\text{aneN}_2\text{S})_2](\text{PF}_6)_2$	2.548(2)	2.160(5)	2.149(5)	[35]
$[\text{Zn}([9]\text{aneN}_2\text{S})_2]\text{ZnCl}_4$	2.550(3)	2.206(6)	2.162(6)	[35]
	2.555(3)	2.159(8)	2.153(7)	

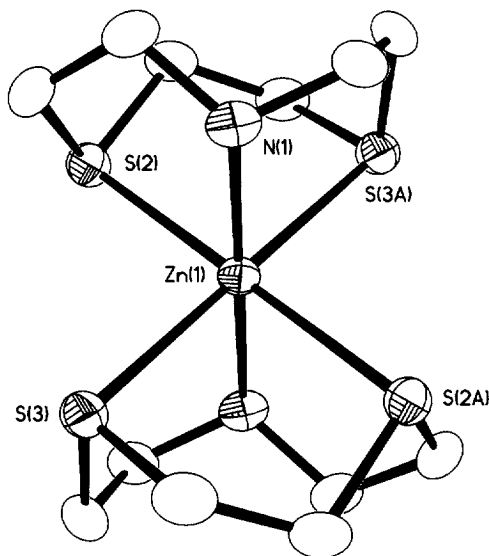


Fig. 28. Structure of  $[\text{Zn}([9]\text{aneNS}_2)_2]^{2+}$ .

A.J. Blake, J.P. Danks, W-S. Li, M. Schröder, unpublished results). The cation consists (Fig. 28) of two macrocycles being bound to the metal in a distorted octahedral geometry. The equatorial plane is occupied by the four thioether donors, with the two aza donors in the axial sites,  $\text{Zn}-\text{N}=2.121(4)$ ,  $\text{Zn}-\text{S}=2.540(1)$ ,  $2.546(1)$  Å.

The reaction of  $\text{HgBr}_2$  with two molar equivalents of  $[9]\text{aneN}_2\text{S} \cdot 2\text{HBr}$  affords  $[\text{Hg}([9]\text{aneN}_2\text{S})_2][\text{HgBr}_4]$  as colourless crystals [75]. The structure shows (Fig. 29)  $\text{Hg}(\text{II})$  in a distorted octahedral geometry, being bound in the equatorial plane by the four N-donors,  $\text{Hg}-\text{N}=2.44(2)$ ,  $2.37(2)$ ,  $2.43(2)$ ,  $2.44(2)$  Å. The axial sites are co-ordinated by two S-donors,  $\text{Hg}-\text{S}=2.724(7)$ ,  $2.74(8)$  Å. Interestingly, the co-ordination geometry is intermediate between octahedral and trigonal prismatic, for reasons that are not clear. This is in contrast to  $[\text{Hg}([9]\text{aneS}_3)_2]^{2+}$  and  $[\text{Hg}([18]\text{aneN}_2\text{S}_4)]^{2+}$  which both exhibit octahedral stereochemistries [77].

#### 4.11. Indium, thallium and lead

The reaction of  $\text{InCl}_3$  with excess  $[9]\text{aneN}_2\text{S} \cdot 2\text{HBr}$  in water affords the complex  $[\text{In}([9]\text{aneN}_2\text{S})]\text{Cl}_2\text{Br}$  [78]. Interestingly, the 2:1 ligand–metal complex could not be isolated. Attempts to produce hydroxo-bridged oligomers by base hydrolysis of  $[\text{In}([9]\text{aneN}_2\text{S})]\text{Cl}_2\text{Br}$  were unsuccessful and resulted in the isolation of  $\text{In}(\text{OH})_3$ . The  $\text{Tl}(\text{I})$  and  $\text{Tl}(\text{III})$  complexes  $[\text{Tl}([9]\text{aneN}_2\text{S})]\text{ClO}_4$  and  $[\text{Tl}([9]\text{aneN}_2\text{S})]\text{Cl}_3$  have been isolated, but no crystallographic data have been reported [78].

Reaction of  $\text{Pb}(\text{OAc})_2$  with  $[9]\text{aneN}_2\text{S}$  and  $\text{KBr}$  gives colourless crystals of  $[\text{Pb}([9]\text{aneN}_2\text{S})]\text{PbBr}_4$  [78], the crystal structure of which shows (Fig. 30) the anion

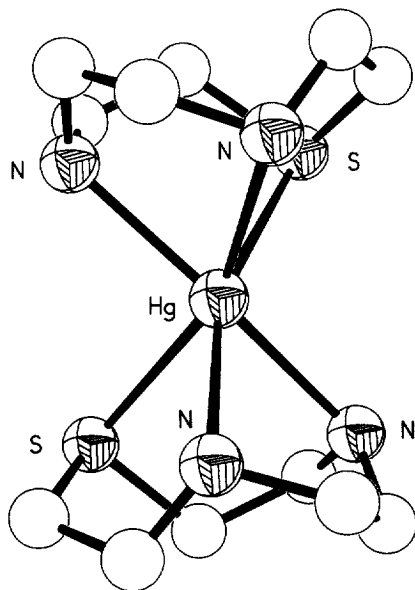


Fig. 29. Structure of  $[\text{Hg}(\text{[9]aneN}_2\text{S})_2]^{2+}$ .

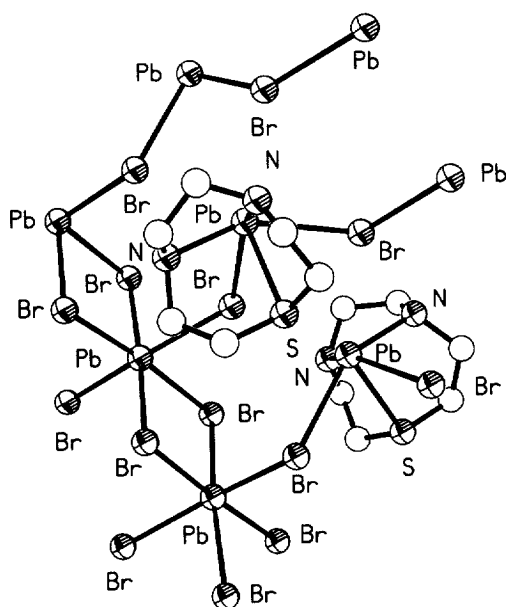


Fig. 30. Structure of  $[\text{Pb}(\text{[9]aneN}_2\text{S})]\text{PbBr}_4$ .

$\text{PbBr}_4^{2-}$  forming continuous chains *via trans* orientated vertices, a structure also found in  $\text{PbCl}_2$  and  $\text{PbBr}_2$  [79]. The macrocycle binds to a  $\text{Pb(II)}$  cation *via* all three donor atoms,  $\text{Pb-N} = 2.544(21)$ ,  $2.549(22)$ ,  $\text{Pb-S} = 2.860(5)$  Å, with the  $\text{Pb(II)}$  centre co-ordinated additionally by a further four  $\text{Br}^-$  anions,  $\text{Pb-Br} = 3.032(3)$ ,  $3.388(4)$ ,  $3.112(3)$ ,  $3.271(4)$  Å, to give an overall co-ordination number of 7 in a “*piano-stool*” geometry.

## 5. N-functionalised tridentate mixed nitrogen and sulfur macrocycles

The reaction of ethyl bromoacetate with [9]ane $\text{N}_2\text{S}$  and [10]ane $\text{N}_2\text{S}$ , followed by hydrolysis yields the *N,N'*-diacetic acid derivatives (TNODA and TDEDA, respectively) [80] (Fig. 31) [75]. The stepwise protonation constants were recorded using standard pH potentiometry, [81] and results are summarised in Table 9. The protonation sequence of the basic sites were obtained using a  $^1\text{H}$  titration profile in which the chemical shifts of the different methylene protons were plotted as a function of the pD. The plots show that the first protonation occurs at the tertiary nitrogen in both ligands whilst the second and third occur at the carboxylate groups.

The stability constants for the formation of 1:1 complexes of TNODA and TDEDA with divalent metal ions have been reported (Table 10) [82]. For comparison the stability constant for the open-chain analogue DMDAESDA is shown (Fig. 32) [82,83]. Many metal ions form complexes with the three ligands except

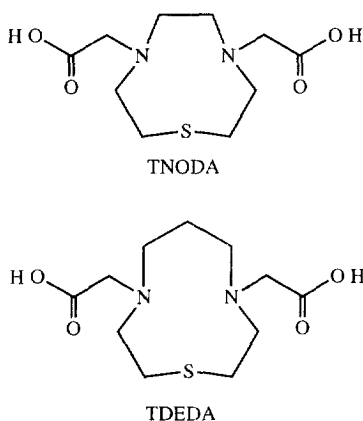


Fig. 31. *N,N'*-diacetic acid derivatives of [9]ane $\text{N}_2\text{S}$  and [10]ane $\text{N}_2\text{S}$ .

Table 9  
Stepwise protonation constants for TNODA and TDEDA

Ligand	$\log K_{\text{H}}^1$	$\log K_{\text{H}}^2$	$\log K_{\text{H}}^3$	$\log K_{\text{H}}^4$	Refs
TNODA	11.63	4.05	2.8		[81]
TDEDA	12.9	3.95	2.0	-0.2	[81]



Table 10

Stability constants of metal-ion complexes of H<sub>2</sub>-TNODA, H<sub>2</sub>-TDEDA and H<sub>2</sub>-DMAESDA (25 °C, *I* = 0.1 mol dm<sup>-3</sup> KNO<sub>3</sub>)

Metal cation	Species	log <i>K</i> <sup>a</sup>		
		TNODA [82]	TDEDA [82]	DMAESDA [82]
Mg(II)	ML	<sup>b</sup>		5.36(4)
	MHL			1.3(1)
Ca(II)	ML	5.01(8)		3.91(7)
	MHL			1.6(1)
	ML <sub>2</sub>			2.5(1)
Sr(II)	ML	3.47(8)		3.05(1)
Ba(II)	ML	2.87(8)		2.66(1)
Mn(II)	ML	9.25(1)	8.97(1)	8.48(2)
	MHL			2.36(8)
Co(II)	ML	13.0(1)	12.0(1)	12.79(1)
Ni(II)	ML	15.60(1) <sup>c</sup>	16.12(2)	15.13(2)
Cu(II)	ML	19.21(1)	22.19(4) <sup>d</sup>	15.73(2)
		18.95(4) <sup>3</sup>	21.93(1) <sup>e</sup>	15.47(2) <sup>e</sup>
	MHL	15.9(2) <sup>e</sup>		
	ML(OH)	2.4(2) <sup>e</sup>		3.87(3) <sup>e</sup>
Zn(II)	ML	14.03(1)	14.41(2)	12.61(3)
	MHL			4.62(5)
	ML(OH)			2.9(1)
Cd(II)	ML	12.99(5)	12.95(2)	10.49(1)
	MHL			3.19(5)
	ML(OH)	4.4(1)		2.44(9)
	M <sub>2</sub> L <sub>2</sub> (OH) <sub>2</sub>	7.0(1)		
Pb(II)	ML	12.96	11.13(9)	11.29(2)
	MHL			3.8(6)
	ML(OH)	1.1(1)		2.82(5)
La(III)	ML	6.02(1)		6.660(3)
	MHL			2.24(6)
	ML <sub>2</sub>			5.10(6)

<sup>a</sup> $K_{ML} = [ML]/[M][L]$ ,  $K_{ML_2} = [ML_2]/[ML][L]$ ,  $K_{MHL} = [MHL]/[M][HL]$ ,  $K_{ML(OH)} = [ML(OH)]/[ML]$  dm<sup>3</sup> mol<sup>-1</sup>,  $K_{M_2L_2(OH)_2} = [M_2L_2(OH)_2]/[ML]^2[OH]^2$  dm<sup>9</sup> mol<sup>-3</sup>; charges are omitted.

<sup>b</sup>No complex formation detected.

<sup>c</sup>At 25 °C, *I* = 1.0 mol dm<sup>-3</sup> KNO<sub>3</sub>.

<sup>d</sup>Estimated value at 0.1 mol dm<sup>-3</sup>.

<sup>e</sup>Estimated value at 1.0 mol dm<sup>-3</sup>.

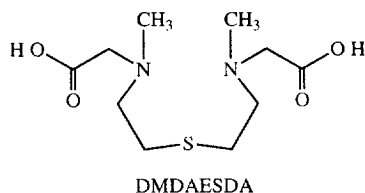
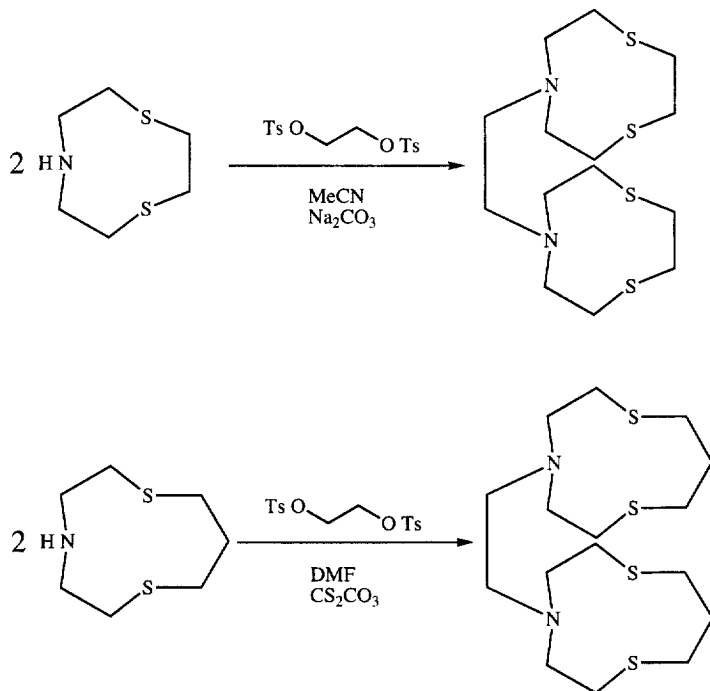


Fig. 32. Open-chain analogue of the *N,N'*-diacetic acid derivatives of [9]aneN<sub>2</sub>S and [10]aneN<sub>2</sub>S.

Mg(II) with TNODA and the alkaline earth metal ions and La(III) with TDEDA. In these cases metal ion complexation was not observed before metal hydroxides were precipitated. The Irving–Williams order of stabilities is observed for all three ligands, while Cu(II), Zn(II) Cd(II) and Pb(II) showed evidence of hydroxo complexes with TNODA, which are not observed for TDEDA.

TNODA and TDEDA show appreciable increase in complex stability over their open-chain analogue DMAESDA. However, when comparing the two macrocyclic derivatives (Table 9) [82] the effect of increasing the macrocycle ring size from nine to a 10-membered ring indicates that TDEDA has a greater complex stability for the smaller metal ions than TNODA, but a decreased stability for the larger metal ions. This is in contrast to the behaviour of [9]aneN<sub>2</sub>S and [10]aneN<sub>2</sub>S (Table 9) where a lower complex stability was observed for [10]aneN<sub>2</sub>S with smaller metal ions. It was concluded [82] that for TNODA and TDEDA the metal ion size based selectivity is controlled by the size of the chelate rings as opposed to macrocyclic ligand size, [83] whereas the reverse is true for [9]aneN<sub>2</sub>S and [10]aneN<sub>2</sub>S [33].

Parker and co-workers have reported [17] the synthesis of an ethyl-linked bis[9]aneNS<sub>2</sub> macrocycle (–CH<sub>2</sub>[9]aneNS<sub>2</sub>)<sub>2</sub> by the reaction of the ditosylate of ethylene glycol with [9]aneNS<sub>2</sub> in MeCN (Scheme 5). The Ag(I) complex of this ligand, [Ag(–CH<sub>2</sub>[9]aneNS<sub>2</sub>)<sub>2</sub>]<sup>+</sup>, has been structurally characterised (Fig. 33) [17,84]. The Ag(I) ion bound to all six donor atoms, with the two macrocyclic



Scheme 5. Synthesis of (–CH<sub>2</sub>[9]aneNS<sub>2</sub>)<sub>2</sub> and (–CH<sub>2</sub>[10]aneNS<sub>2</sub>)<sub>2</sub>.

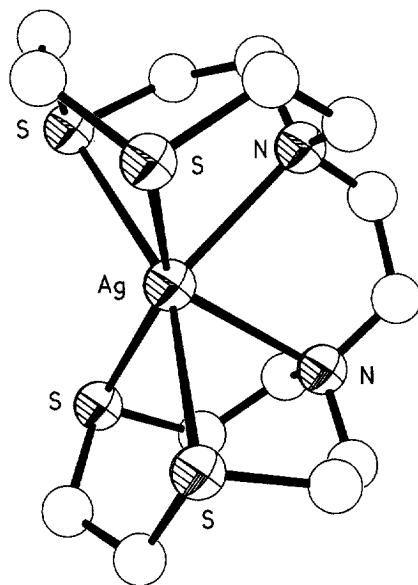
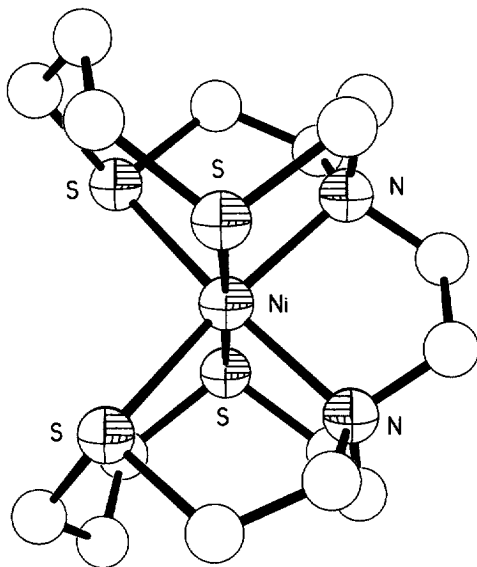
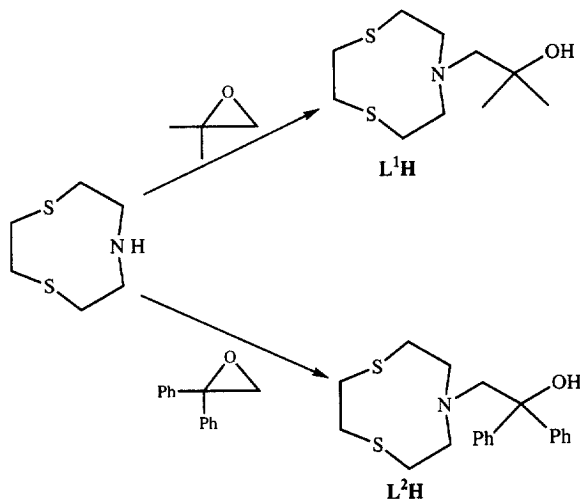


Fig. 33. Structure of  $[\text{Ag}(-\text{CH}_2[9]\text{aneNS}_2)_2]^+$ .

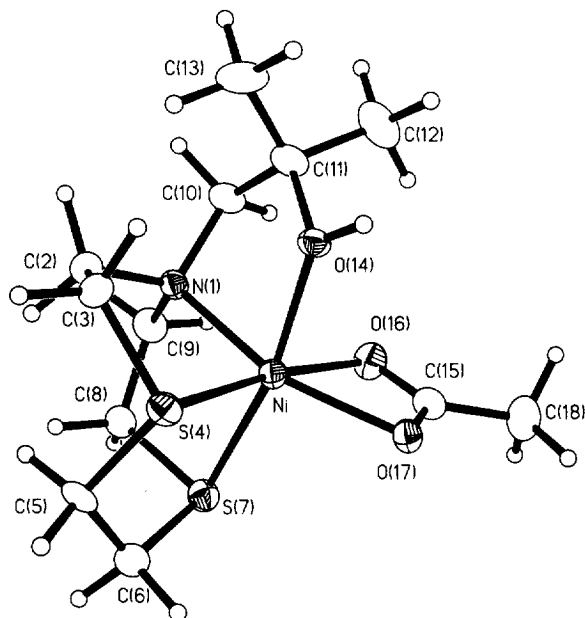
fragments co-ordinating facially to the metal ion. There is a relatively short Ag–N bond of 2.586(3) Å, one short Ag–S bond of 2.611(2) Å, and a longer Ag–S bond of 2.802(2) Å. The Ag(I) centre is in a very distorted octahedral geometry, in which the donor sets of macrocycle are twisted 17° relative to one another. The authors conclude that this distortion is probably due to the bridging ethylene group being too short for the two macrocyclic rings to adopt a more regular octahedral geometry to the metal cation. Also, the small size of the macrocycles is probably more suited for binding smaller cations.

McAuley and co-workers have synthesised [48] the related ethyl-linked bis[10]aneNS<sub>2</sub> ligand  $(-\text{CH}_2[10]\text{aneNS}_2)_2$  using a similar route to Parker's ethyl-linked bis[9]aneNS<sub>2</sub> system. The corresponding Ni(II) complex  $[\text{Ni}(-\text{CH}_2[10]\text{aneNS}_2)_2]^{2+}$  shows (Fig. 34) the Ni(II) ion to be in a very distorted octahedral environment, being bound to all six donors, Ni–S=2.389(2), 2.415(2), Ni–N=2.112(5) Å. The twist imposed by the ethylene bridge is 20° and is halfway to a trigonal prismatic geometry. One interesting difference between this complex and  $[\text{Ni}([10]\text{aneNS}_2)_2]^{2+}$  is that in the latter the two N-donors are *trans* to one another, whereas in the ethylene bridged [10]aneNS<sub>2</sub> this conformation is not possible and the N-donors are therefore *cis* to one another.

The reaction of isopropylene oxide and 1-1-diphenylethylene oxide with [9]aneNS<sub>2</sub> affords the corresponding pendant arm tertiary alcohol derivatives L<sup>1</sup>H and L<sup>2</sup>H, (Scheme 6) [21,85]. Complexation of L<sup>1</sup>H with Ni(OAc)<sub>2</sub> gave a deep-blue crystalline complex  $[\text{Ni}(\text{L}^1\text{H})(\text{OAc})]\text{BPh}_4 \cdot \text{MeCN}$ , the crystal structure of which (Fig. 35) reveals the Ni(II) centre to be co-ordinated to all three donors of the

Fig. 34. Structure of  $[\text{Ni}(-\text{CH}_2[10]\text{aneNS}_2)_2]^{2+}$ .Scheme 6. Synthesis of  $\text{L}^1\text{H}$  and  $\text{L}^2\text{H}$ .

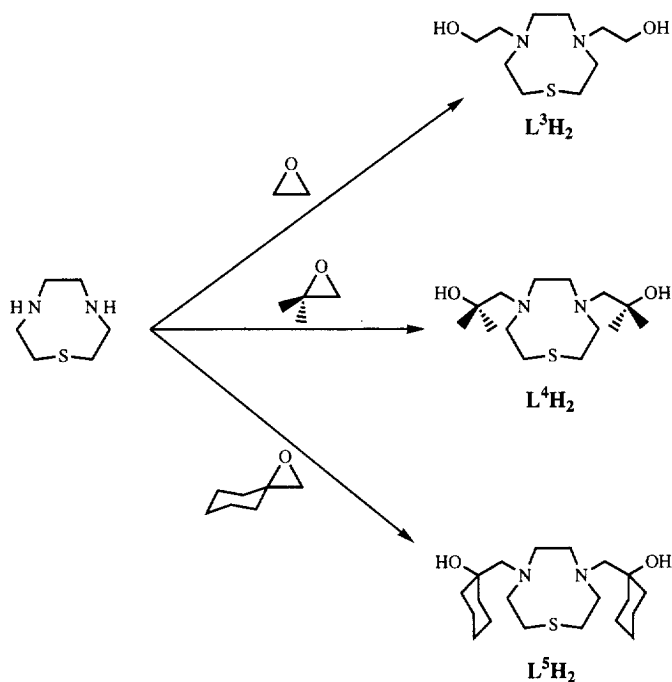
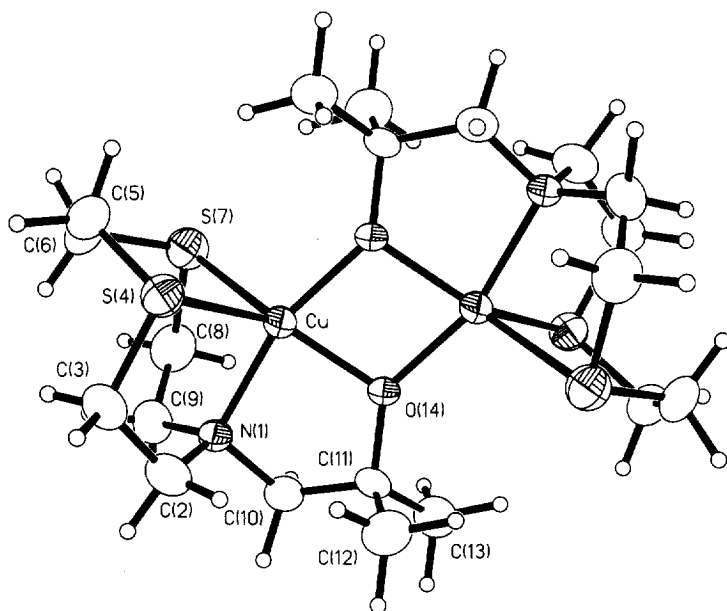
macrocyclic,  $\text{Ni}-\text{N}=2.064(3)$ ,  $\text{Ni}-\text{S}=2.3658(12)$ ,  $2.3875(13)$  Å. The pendant arm co-ordinates to the metal centre as an alcohol,  $\text{Ni}-\text{OH}=2.061(3)$  Å, and the co-ordination sphere completed by an  $\text{AcO}^-$  chelate. The  $\text{Ni}(\text{II})$  centre is in a distorted octahedral geometry, being partly due to the bidentate acetate ligand, which has a small bite angle,  $\text{O}(16)-\text{Ni}-\text{O}(17)=62.86^\circ$  [21]. The inclusion of a

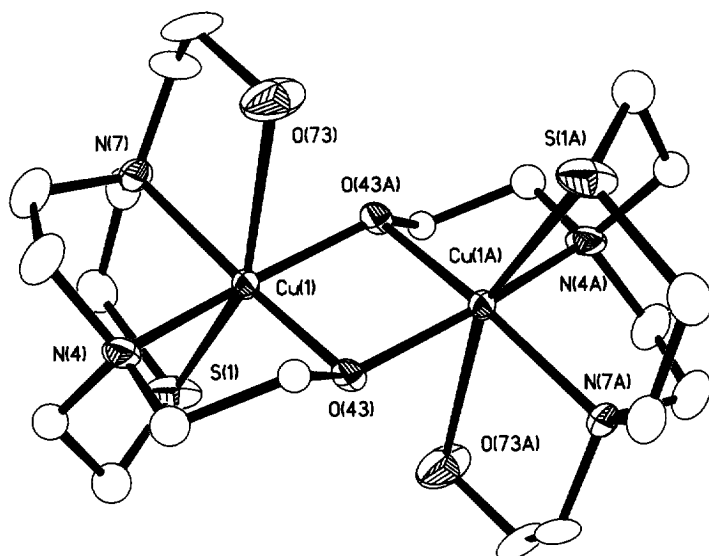
Fig. 35. Structure of  $[\text{Ni}(\text{L}^1\text{H})(\text{OAc})]^+$ .

chelating acetate is unusual as it is more commonly found as bridging ligands between two metal centres [86].

The dimeric complex  $[\text{Cu}_2(\text{L}^1)^2](\text{BPh}_4)_2$  (Fig. 36) reveals the macrocycle to be co-ordinated facially to the Cu(II) centre,  $\text{Cu}-\text{N}(1)=2.042(4)$ ,  $\text{Cu}-\text{S}(4)=2.4519(15)$ ,  $\text{Cu}-\text{S}(7)=2.4305(16)$  Å. The pendant arm is deprotonated to give an alkoxide which bridge two metal centres  $\text{Cu}-\text{O}(14)=1.927(4)$  Å. The Cu(II) centres are in a distorted trigonal bipyramidal geometry with S(4), S(7) and O(14) lying in the equatorial plane and N(1) and O(14') in the axial positions. The Cu–O–Cu' angle is  $102.73^\circ$ . The magnetochemistry of the complex gave a coupling constant of  $2J = -220 \text{ cm}^{-1}$ , indicating antiferromagnetic coupling, although the authors noted that the material was contaminated with 9% paramagnetic impurities, which could not be removed even after repeated recrystallisations [21].

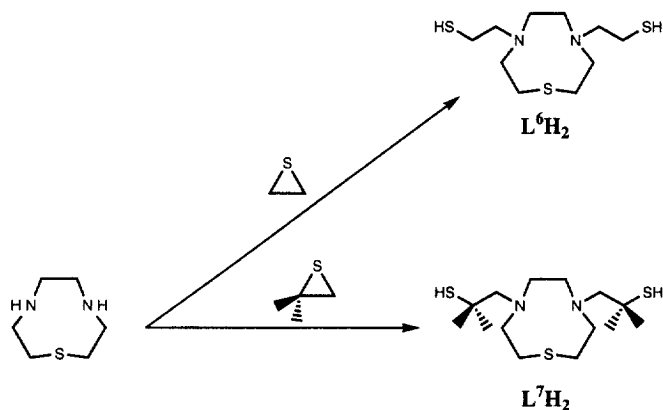
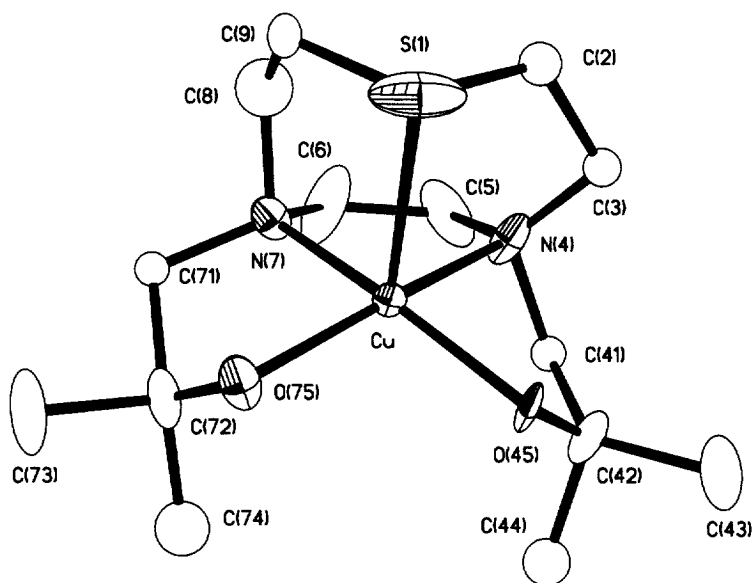
Schröder and co-workers have synthesised the pendant arm alcohol derivatives of [9]aneN<sub>2</sub>S, L<sup>3</sup>H<sub>2</sub>, L<sup>4</sup>H<sub>2</sub> and L<sup>5</sup>H<sub>2</sub> (Scheme 7), with a view to monitoring the effects of increasing the steric bulk of the pendant arm has upon the Cu(II) complexes [87]. All three ligands afford the Cu(II) complexes as their PF<sub>6</sub><sup>−</sup> salts. The Cu(II) complex of L<sup>3</sup>H<sub>2</sub> was found to be the dimeric compound  $[\text{Cu}_2(\text{L}^3\text{H})_2](\text{PF}_6)_2$  (Fig. 37) in which each macrocycle is bound to a Cu(II) centre in a facial manner,  $\text{Cu}(1)-\text{N}(4)=2.005(6)$ ,  $\text{Cu}(1)-\text{N}(7)=2.043(6)$ ,  $\text{Cu}-\text{S}(1)=2.648(2)$  Å. One of the pendant arms from each ligand forms an alcohol linker to one copper centre,  $\text{Cu}(1)-\text{O}(73)=2.757(6)$  Å. The remaining two pendant arms are deprotonated and form an alkoxide bridge between the metal centres,

Scheme 7. Synthesis of  $\text{L}^3\text{H}_2$ ,  $\text{L}^4\text{H}_2$  and  $\text{L}^5\text{H}_2$ .Fig. 36. Structure of  $[\text{Cu}_2(\text{L}^1)_2]^{2+}$ .

Fig. 37. Structure of  $[\text{Cu}_2(\text{L}^3\text{H})_2]^{2+}$ .

$\text{Cu}(1)–\text{O}(43)=1.931(4)$  Å. The metal centres are Jahn–Teller distorted octahedra with the two N donors from the macrocycle and the two alkoxide bridges in close equatorial positions with the relatively poorer  $\sigma$ -donor alcohol and S-donor of  $[\text{9}]_{\text{ane}}\text{N}_2\text{S}$  at pseudo axial positions. The  $\text{Cu}\cdots\text{Cu}$  distance is  $2.941(2)$  Å, and the  $\text{Cu}–\text{O}–\text{Cu}$  bond angle is  $98.94^\circ$ . The magnetochemistry of  $[\text{Cu}_2(\text{L}^3\text{H})_2](\text{PF}_6)_2$  ( $J=0.0006\text{ cm}^{-1}$ ) indicates that the two  $\text{Cu}(\text{II})$  centres are acting independently of one another and there is little or no exchange between the centres [87]. With  $\text{L}^4\text{H}_2$  two complexes were isolated, both the dimeric and the monomeric species,  $[\text{Cu}_2(\text{L}^4\text{H})_2](\text{PF}_6)_2$  and  $[\text{Cu}(\text{L}^4\text{H})]\text{PF}_6$ , respectively. Only the monomeric species has been crystallised and the structure is shown in Fig. 38. The  $\text{Cu}(\text{II})$  centre is five co-ordinate with the two N-donors the alcohol and the alkoxide of the pendant arms in the equatorial positions, and the S-atom forming a long apical interaction,  $\text{Cu}–\text{S}(1)=2.502(4)$ ,  $\text{Cu}–\text{N}(4)=2.037(9)$ ,  $\text{Cu}–\text{N}(7)=2.031(10)$ ,  $\text{Cu}–\text{O}(45)=1.938(10)$ ,  $\text{Cu}–\text{O}(75)=1.948(9)$  Å [87]. Surprisingly, both the  $\text{Cu}(\text{II})$  bond lengths to the hydroxo and the alkoxide are approximately the same, which is probably due to the disorder within the structure scrambling these positions. The addition of  $\text{Cu}(\text{NO}_3)_2 \cdot 3\text{H}_2\text{O}$  to  $\text{L}^5\text{H}_2$  yields only one product, which has not been successfully crystallised, although UV–visible spectroscopic and mass spectrometric data indicate the product to be the monomeric complex  $[\text{Cu}(\text{L}^5\text{H})]\text{PF}_6$ . In conclusion, the introduction of bulky pendant arms inhibits dimer formation and encourages the production of monomeric complexes [88].

Schröder and co-workers have treated  $[\text{9}]_{\text{ane}}\text{N}_2\text{S}$  with ethylene sulfide and isopropylene sulfide to isolate the bis thiol ligands  $\text{L}^6\text{H}_2$  and  $\text{L}^7\text{H}_2$  (Scheme 8) and have isolated the  $\text{Ni}(\text{II})$  complexes,  $[\text{Ni}_3(\text{L}^6)_2](\text{BF}_4)_2$  (Fig. 39) and  $[\text{Ni}_3(\text{L}^7)_2](\text{BF}_4)_2$

Scheme 8. Synthesis of  $L^6H_2$  and  $L^7H_2$ .Fig. 38. Structure of  $[Cu(L^4H)_2]^{2+}$ .

(Fig. 40), respectively [89]. Both complexes are isostructural having a 3:2 M:ligand stoichiometry. In the case of  $[Ni_3(L^7)_2]2BF_4$  (Fig. 40) the two nitrogen atoms and the sulfur atom of the macrocyclic ring facially cap the Ni(II) centre with  $Ni(1)-N(14)=1.946(7)$ ,  $Ni(1)-N(17)=1.972(7)$ ,  $Ni(1)-S(11)=2.584(3)$  Å. The two thiol pendant arms are deprotonated and form thiolate linkages to the metal centre with bond distances,  $Ni(1)-S(14)=2.167(3)$  and  $Ni(1)-S(17)=2.153(3)$  Å respectively. Ni(1) is in a square pyramidal geometry with the two nitrogen and two thiolate donors in the equatorial sites, whilst the softer S-donor of the macrocycle



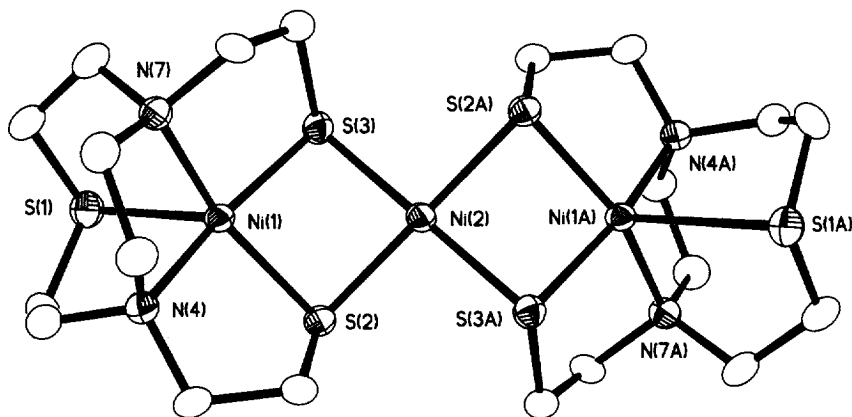


Fig. 39. Structure of  $[\text{Ni}_3(\text{L}^6)_2]^{2+}$ .

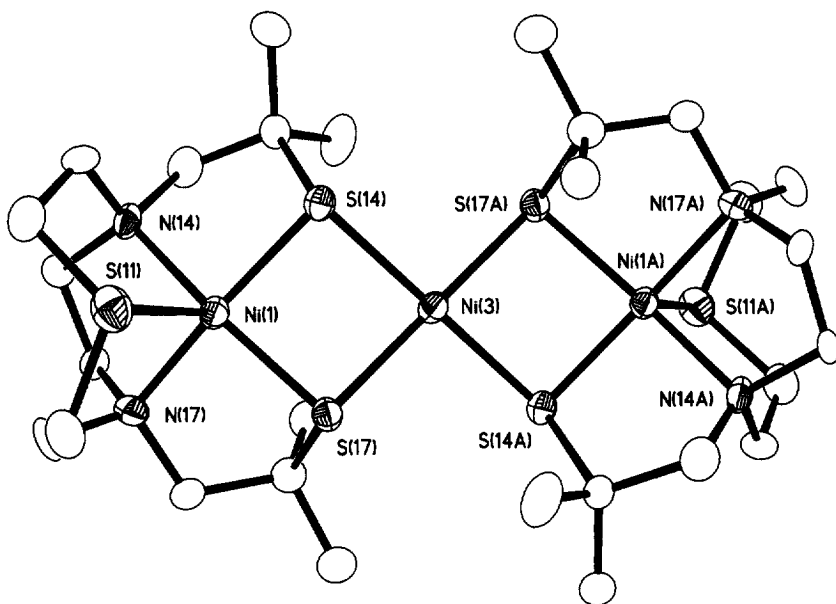
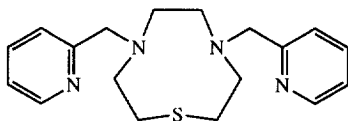
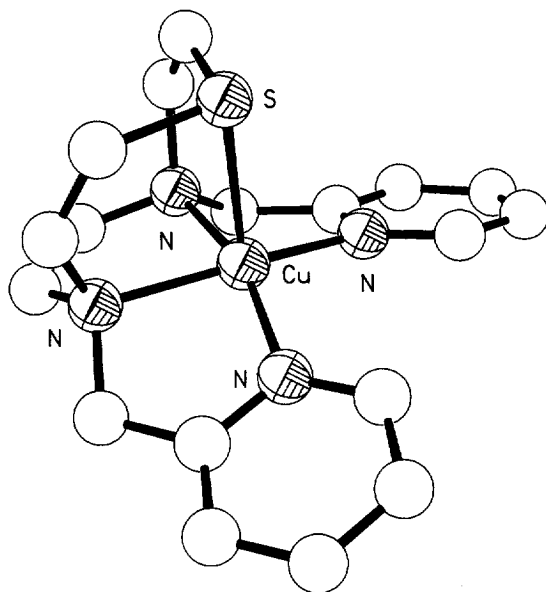


Fig. 40. Structure of  $[\text{Ni}_3(\text{L}^7)_2]^{2+}$ .

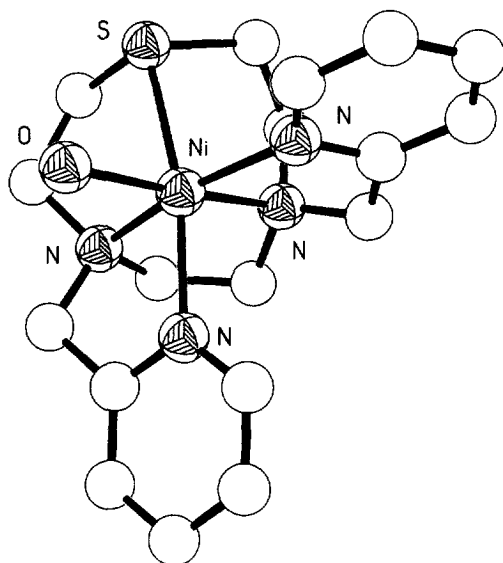
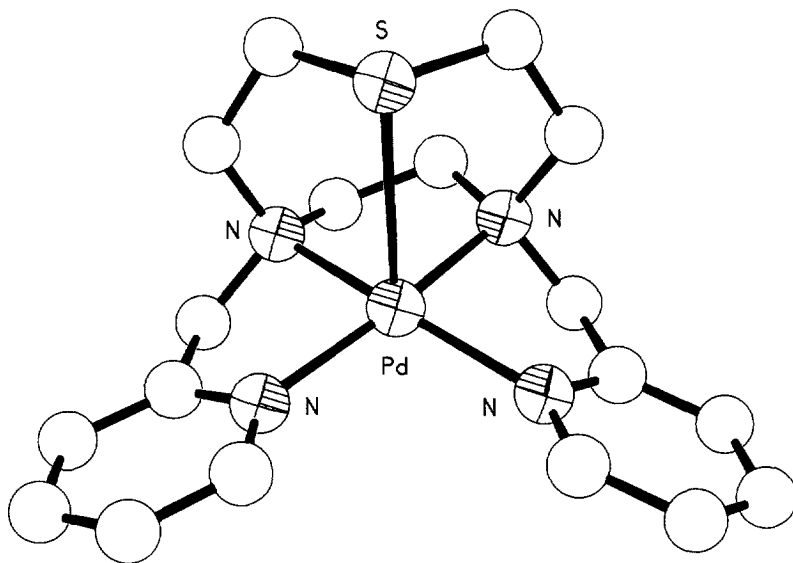
takes up the axial position. Two of these Ni(II) macrocyclic fragments are joined together via the thiolate functionalities to a third Ni (II) cation in a square planar geometry, with metal to thiolate bond distances in the range 2.220–2.259(2) Å [89].

The synthesis of [9]aneN<sub>2</sub>S with two pendant pyridyl arms (L<sup>8</sup>) (Fig. 41) has been published by two groups using similar procedures [90–92]. The X-ray crystal structures of the Cu(II) [90], Ni(II) [91], Pd(II) [91,92] and Pt(II) [91] complexes (Figs. 42–45, respectively) have been determined. [Cu(L<sup>8</sup>)](ClO<sub>4</sub>)<sub>2</sub> is five co-ordinate

Fig. 41.  $N,N'$ - $\{\text{CH}_2(2\text{-py})\}_2\text{-[9]aneN}_2\text{S L}^8$ .Fig. 42. Structure of  $[\text{Cu}(\text{L}^8)]^{2+}$ .

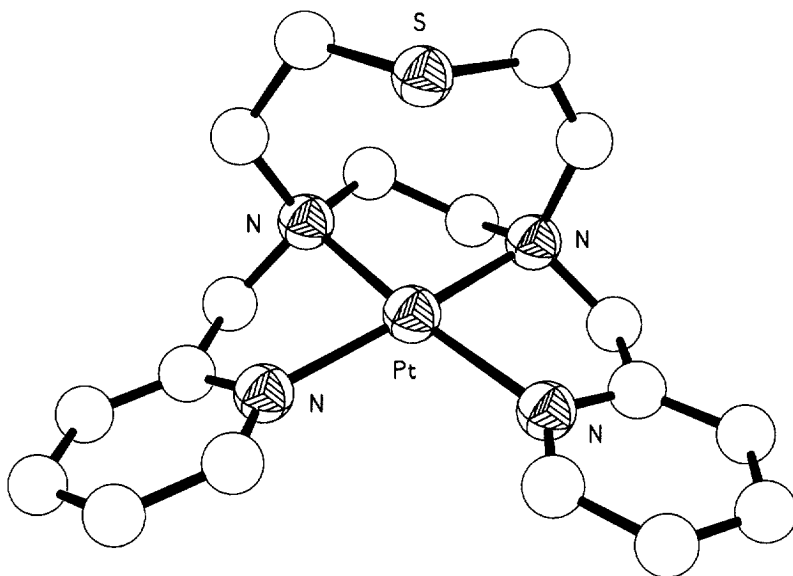
with a square pyramidal geometry, the two macrocyclic N-donors and the two pyridyl N-donors are in the equatorial positions,  $\text{Cu-N} = 2.037(8)$ ,  $2.037(8)$ ,  $2.005(8)$ ,  $2.005(8)$  Å respectively, while the S-donor is at the axial site,  $\text{Cu-S} = 2.496(8)$  Å, and a  $\text{ClO}_4^-$  anion interacts weakly with the Cu(II) centre,  $\text{Cu-O} = 2.955(6)$  Å. The Cu(II) atom lies out of the basal plane towards the S donor by 0.22 Å. The cations  $[\text{Pd}(\text{L}^8)]^{2+}$  [91,92] and  $[\text{Pt}(\text{L}^8)]^{2+}$  [91] exhibit very similar co-ordination geometry to  $[\text{Cu}(\text{L}^8)]^{2+}$ , the M–S distances to the axial S-donor being much longer than that found in the Cu(II) structure as expected for  $d^8$  metal centres,  $\text{Pd-S} = 2.907(1)$  [91],  $\text{Pd-S} = 2.915(3)$  [92],  $\text{Pt-S} = 3.056(3)$  Å [91].

The addition of  $\text{Ni}(\text{ClO}_4)_2$  to  $\text{L}^8$  affords the complex  $[\text{Ni}(\text{L}^8)(\text{H}_2\text{O})](\text{ClO}_4)_2$  [91], the structure of which reveals (Fig. 43) an octahedral geometry for Ni(II), with the macrocycle facially capping Ni(II),  $\text{Ni-S} = 2.393(5)$ ,  $\text{Ni-N} = 2.069(13)$ ,  $2.088(13)$  Å. The co-ordination is completed by the two pyridyl donors and a water molecule,  $\text{Ni-N} = 2.098(12)$ ,  $2.030(13)$ ,  $\text{Ni-O} = 2.103(11)$  Å, respectively. In contrast to the Cu(II), Pd(II) and the Pt(II) structures where the square plane is provided by the four donor N atoms of ligand, the basal plane is made up from the two macrocyclic N donors, one of the pyridyl pendant arm N-donors and the water

Fig. 43. Structure of [Ni(L<sup>8</sup>)(H<sub>2</sub>O)]<sup>2+</sup>.Fig. 44. Structure of [Pd(L<sup>8</sup>)]<sup>2+</sup>.

oxygen. The axial sites are provided by the S-donor of the macrocycle and the remaining pyridyl N-donor.

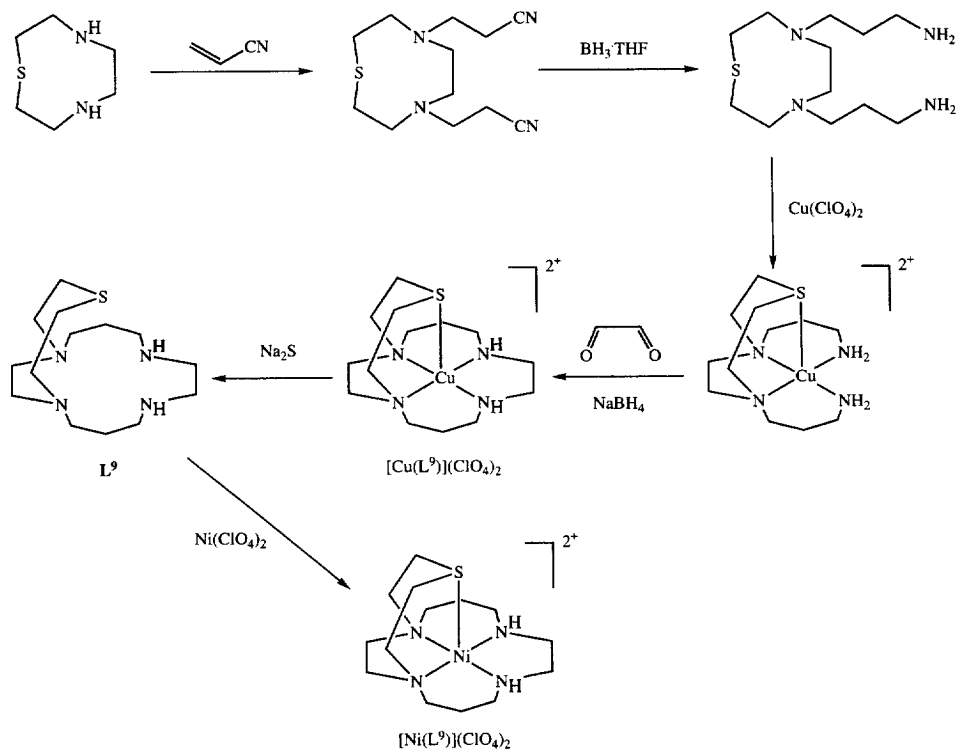
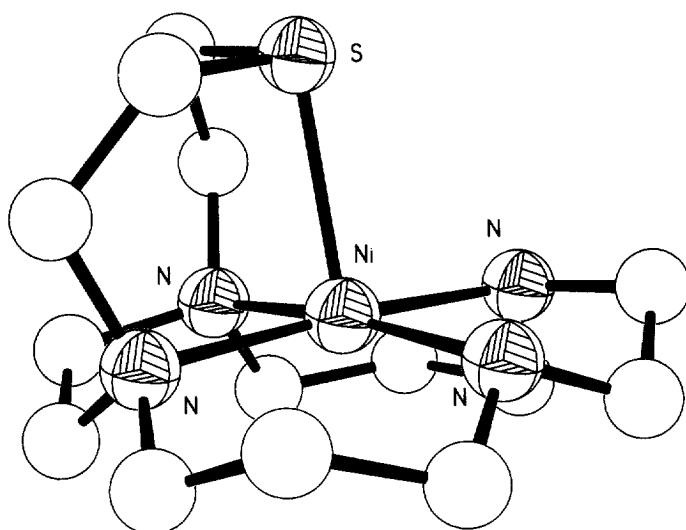
A very elegant synthesis of a novel macrobicyclic ligand incorporating the [9]aneN<sub>2</sub>S fragment has been reported (FScheme 9) [93]. The synthesis takes advan-

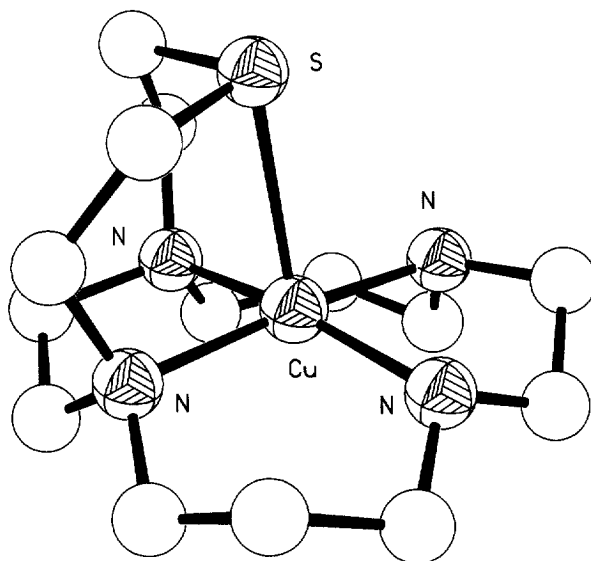
Fig. 45. Structure of  $[\text{Pt}(\text{L}^8)]^{2+}$ .

tage of a metal template ring-closure [94], where the Cu(II) centre promotes the ring closure step with glyoxal ( $\text{OHCCHO}$ ) to form Schiff base intermediate which is reduced in situ by  $\text{BH}_3 \cdot \text{THF}$  to yield the macrobicyclic system. Removal of the templating metal yields the free ligand  $\text{L}^9$ . It is worth noting that this is the first successful attempt at using a copper ion for the template synthesis of a cyclam ( $[\text{14}] \text{aneN}_4$ ) derivative with glyoxal. Cyclam can not be prepared using a copper-promoted ring-closure with glyoxal as copper metal is precipitated in the reduction step with  $\text{BH}_3 \cdot \text{THF}$  [95]. In preparing  $\text{L}^9$ , however, the Cu(II) complex is five co-ordinate and the authors conclude that this could possibly lead to the stabilisation of the intermediate formed in the cyclisation process with glyoxal [93].

The complexes  $[\text{Ni}(\text{L}^9)](\text{ClO}_4)_2$  and  $[\text{Cu}(\text{L}^9)](\text{ClO}_4)_2$  have been structurally characterised (Figs. 46 and 47). Both complexes show similar co-ordination geometries. The cyclam portion of the ligand complexes to the metal ions with all four N-donor atoms in equatorial positions. The sulfur atom co-ordinates axially, the S–M vector and the  $\text{N}_4$  plane shows a small aberration from the perpendicular, the angles between S–M and the  $\text{N}_4$  plane being  $81.8^\circ$  and  $83.5^\circ$  for  $[\text{Ni}(\text{L}^9)](\text{ClO}_4)_2$  and  $[\text{Cu}(\text{L}^9)](\text{ClO}_4)_2$ , respectively. The authors suggest that this is because the  $[\text{9}] \text{aneN}_2\text{S}$  portion of the ligand cannot reach over to encapsulate the axial site.  $[\text{Ni}(\text{L}^9)](\text{ClO}_4)_2$  has a  $\text{ClO}_4^-$  anion forming a close interaction to the Ni(II) cation,  $\text{Ni} \cdots \text{O} = 2.563(6) \text{ \AA}$ .  $[\text{Cu}(\text{L}^9)](\text{ClO}_4)_2$  however, shows a much weaker interaction to a perchlorate ion  $\text{Cu} \cdots \text{O} = 3.140 \text{ \AA}$ , which the authors describe as an electrostatic rather than a bonding interaction [93].

In aqueous solution the complex  $[\text{Cu}(\text{L}^9)](\text{ClO}_4)_2$  complex remains five co-ordinate while the complex  $[\text{Ni}(\text{L}^9)](\text{ClO}_4)_2$  is six co-ordinate, with a water molecule taking

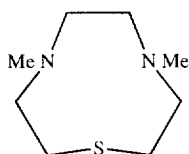
Scheme 9. Synthesis of  $L^9\text{H}$ ,  $[\text{Cu}(\text{L}^9)](\text{ClO}_4)_2$  and  $[\text{Ni}(\text{L}^9)](\text{ClO}_4)_2$ .Fig. 46. Structure of  $[\text{Ni}(\text{L}^9)]^{2+}$ .

Fig. 47. Structure of  $[\text{Cu}(\text{L}^9)]^{2+}$ .

up the sixth site. ESR spectra of the Cu(II) complex and the chemically generated Ni(III) complexes are typical for five and six co-ordinate metal complexes, respectively. Cyclic voltammetry of the Cu(II) complex shows a reversible Cu(II)/Cu(I) couple at  $E_{1/2} = -0.935$  V indicating that the  $[\text{Cu}(\text{L}^9)]^+$  is a strong reductant. This value is 400–500 mV less reducing than  $[\text{Cu}(\text{cyclam})]^+$  [96] reflecting the  $\pi$ -acceptor properties of the sulfur centre in  $\text{L}^9$ .

$[\text{9}] \text{aneN}_2\text{S}$  has been dimethylated by a known route for the methylation of secondary amines [97] to give the ligand  $\text{Me}_2[\text{9}] \text{aneN}_2\text{S}$  (Fig. 48) [43]. The complex  $[\text{Fe}(\text{Me}_2[\text{9}] \text{aneN}_2\text{S})\text{Cl}_3]$  has been structurally characterised and is isostructural to the complex  $[\text{Fe}([\text{9}] \text{aneN}_2\text{S})\text{Cl}_3]$ . [43] There is a slight elongation in the Fe–N bond distance (0.08 Å) on going from  $[\text{Fe}([\text{9}] \text{aneN}_2\text{S})\text{Cl}_3]$  to  $[\text{Fe}(\text{Me}_2[\text{9}] \text{aneN}_2\text{S})\text{Cl}_3]$ , but this distance is still shorter than in  $[\text{Fe}(\text{Me}_2[\text{9}] \text{aneN}_3)\text{Cl}_3]$  [98].

The reaction of  $[\text{Fe}(\text{Me}_2[\text{9}] \text{aneN}_2\text{S})\text{Cl}_3]$  with NaOAc, followed by anion metathesis, affords the binuclear complex,  $[\text{Fe}_2\text{O}(\text{O}_2\text{CMe})_2(\text{Me}_2[\text{9}] \text{aneN}_2\text{S})_2](\text{PF}_6)_2$  [43]. The crystal structure shows two  $[\text{Fe}(\text{Me}_2[\text{9}] \text{aneN}_2\text{S})]^{3+}$  moieties linked by two acetate and an oxo ligand. The structure reveals that the thioether units are *cis* with respect to the bridging oxo unit and in a *gauche* configuration with respect to the

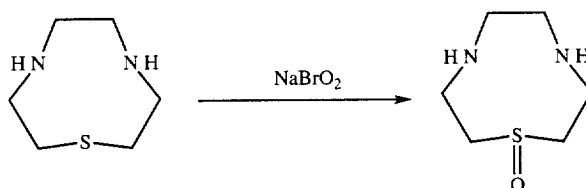
Fig. 48.  $\text{Me}_2[\text{9}] \text{aneN}_2\text{S}$ .

Fe–O–Fe plane. This is in contrast to  $[\text{Fe}_2\text{O}(\text{O}_2\text{CMe})_2([\text{9}] \text{aneN}_2\text{S})_2](\text{PF}_6)_2$ , in which the thioether units are *trans* with respect to the bridging oxo unit and in a *syn* configuration with respect to the Fe–O–Fe plane [43]. The Fe–Fe distance is 0.019(3) Å longer in  $[\text{Fe}_2\text{O}(\text{O}_2\text{CMe})_2(\text{Me}_2[\text{9}] \text{aneN}_2\text{S})_2](\text{PF}_6)_2$  reflecting the extra steric bulk upon methylation of [9]aneN<sub>2</sub>S. This is not such a marked effect as for the [9]aneN<sub>3</sub> analogues which show an increase in the Fe–Fe distance of 0.057(5) on going from  $[\text{Fe}_2\text{O}(\text{O}_2\text{CMe})_2([\text{9}] \text{aneN}_3)_2](\text{PF}_6)_2$  to  $[\text{Fe}_2\text{O}(\text{O}_2\text{CMe})_2(\text{Me}_3[\text{9}] \text{aneN}_3)_2](\text{PF}_6)_2$  [99, 100].

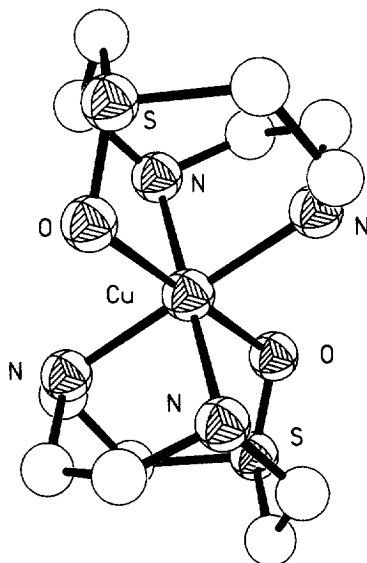
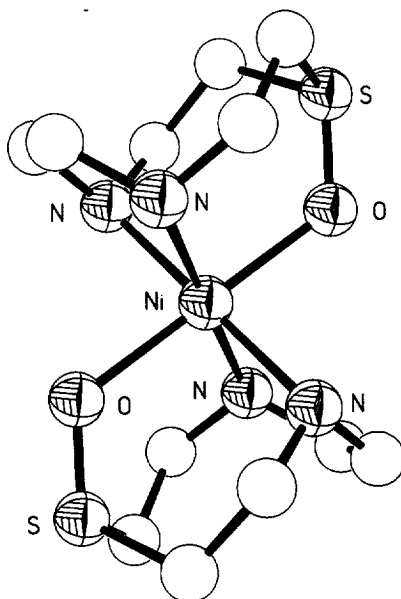
## 6. S-functionalised tridentate mixed nitrogen and sulfur macrocycles

[9]aneN<sub>2</sub>S has been treated with sodium bromite to oxidise the thioether S to a sulfoxide [101] to give the ligand L<sup>10</sup> (Scheme 10). A range of Co(III), Ni(II) and Cu(II) complexes  $[\text{M}(\text{L}^{10})_2]^{x+}$  have been prepared and spectroscopic evidence indicates that the sulfoxide group is co-ordinated through the oxygen atom and that the complexes have a *trans*-O,O geometry. Subsequently, the complexes  $[\text{Cu}(\text{L}^{10})_2]\text{Br}_2$ ,  $[\text{Ni}(\text{L}^{10})_2](\text{ClO}_4)_2$ ,  $[\text{Pd}(\text{L}^{10})_2]\text{Br}_2$  and  $[\text{Pt}(\text{L}^{10})_2]\text{Br}_2$  have been prepared and structurally characterised [102]. In the complex  $[\text{Cu}(\text{L}^{10})_2]\text{Br}_2$  (Fig. 49) the Cu(II) sits on an inversion centre, and is in a distorted octahedral geometry being bound by the four N-donors in the equatorial plane, Cu–N = 2.017(3), 2.043(3) Å and two O-donors of the sulfoxides in the axial positions, Cu–O = 2.369(3) Å. The long apical interactions clearly indicate a Jahn–Teller distortion within the complex.

The complex  $[\text{Ni}(\text{L}^{10})_2](\text{ClO}_4)_2$  shows (Fig. 50) a similar co-ordination geometry to the Cu(II) complex, the Ni(II) centre being bound by the four N-donors in the equatorial plane Ni–N = 2.12(1), 2.15(1) Å and the O-donors in the axial sites, Cu–O = 2.067(7) Å. Interestingly, in the case of the acyclic analogue  $[\text{Ni}(\text{L}^{11})_2]^{2+}$  (L<sup>11</sup> = 3-thia-1,5-diaminopentane-S-oxide, Fig. 51) the two O-donors are in a mutually *cis* geometry [101]. The reasons for the difference in co-ordination mode for complexes of L<sup>10</sup> and L<sup>11</sup> with Ni(II) are not clear, although the authors suggest that steric restrictions within the ligands and interactions between the donor atoms and the Ni(II) centre may be a factor. This is exactly parallel to the complexes  $[\text{Ni}([\text{9}] \text{aneN}_2\text{S})_2]^{2+}$  [12] and its analogous open-chain complex  $[\text{Ni}(\text{daes})_2]^{2+}$  [54]. In the case of  $[\text{Ni}([\text{9}] \text{aneN}_2\text{S})_2]^{2+}$  the S-donors are *trans* to one another while in  $[\text{Ni}(\text{daes})_2]^{2+}$  they are mutually *cis*.

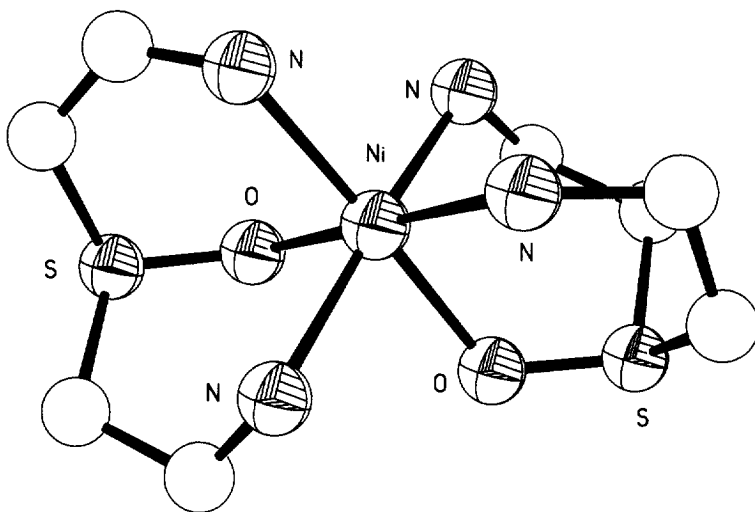
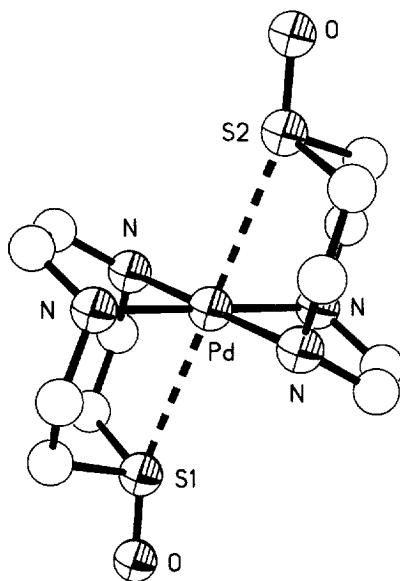


Scheme 10. Synthesis of (L<sup>10</sup>).

Fig. 49. Structure of  $[\text{Cu}(\text{L}^{10})_2]^{2+}$ .Fig. 50. Structure of  $[\text{Ni}(\text{L}^{10})_2]^{2+}$ .

The cation  $[\text{Pd}(\text{L}^{10})_2]^{2+}$  [101] is on a crystallographic inversion centre with the Pd(II) being bound by the four N-donors in a square planar co-ordination geometry (Fig. 52), Pd–N = 2.050(5) Å. There are long-range interactions to the S-donors of



Fig. 51. Structure of  $[\text{Ni}(\text{L}^{11})_2]^{2+}$ .Fig. 52. Structure of  $[\text{Pt}(\text{L}^{10})_2]^{2+}$ .

the sulfoxide groups,  $\text{Pd-S} = 2.981(4) \text{ \AA}$ . In contrast,  $[\text{Pt}(\text{L}^{10})_2]^{2+}$  has a square planar arrangement  $\text{Pt-N} = 2.05(1)$  and  $2.06(6) \text{ \AA}$ , though in this case the sulfoxide donors are pointing away from the metal centre and are not interacting with the  $\text{Pt(II)}$ . This parallels the complexes  $[\text{Pd}([9]\text{aneN}_2\text{S})_2](\text{PF}_6)_2$  [56,57]

and  $[\text{Pt}([9]\text{aneN}_2\text{S})_2](\text{PF}_6)_2$  [57] where, in the case of the Pd(II) complex there are long-range apical interactions to the metal centre, but not in the Pt(II) complex.

## 7. Concluding remarks

The ligands  $[9]\text{aneN}_2\text{S}$ ,  $[9]\text{aneNS}_2$  and their derivatives are finding increasing importance as face-capping ligands that complement the chemistries of their homoleptic congeners  $[9]\text{aneS}_3$  and  $[9]\text{aneN}_3$ . The resultant stable complexes show novel stereochemical and redox properties based upon the complementarity of these small-ring ligands (macrocyclic effect) with the ionic radii of first row and related hard and soft transition metal ions. Future work is likely to focus on these ligands and their pendant-arm derivatives as mixed hard–soft donor ligands for modelling bio-sites in metalloproteins, and in metal-extraction, -recognition, -sensing and -selectivity studies.

## References

- [1] W. Rosen, D.H. Busch, *J. Chem. Soc. Chem. Commun.* (1969) 148.
- [2] W. Rosen, D.H. Busch, *J. Am. Chem. Soc.* 91 (1969) 4969.
- [3] W. Rosen, D.H. Busch, *Inorg. Chem.* 9 (1970) 262.
- [4] N.R. Champness, J.P. Danks, M. Schröder, in preparation.
- [5] A.J. Blake, M. Schröder, *Advances Inorg. Chem.* 35 (1990) 1.
- [6] S.C. Rawle, S.R. Cooper, *Struct. Bonding (Berlin)* 72 (1990) 1.
- [7] S.G. Murray, F.R. Hartley, *Chem. Rev.* 81 (1981) 356.
- [8] A.J. Blake, A.J. Holder, T.I. Hyde, M. Schröder, *J. Chem. Soc., Chem. Commun.* (1989) 1433.
- [9] P. Chaudhuri, K. Wieghardt, *Prog. Inorg. Chem.* 35 (1987) 329.
- [10] L.R. Gahan, G.A. Lawrence, A.M. Sargeson, *Aust. J. Chem.* 35 (1982) 1119.
- [11] L.R. Gahan, T.W. Hambley, A.M. Sargeson, *Inorg. Chem.* 21 (1982) 2699.
- [12] S.M. Hart, J.C.A. Boeyens, J.P. Michael, R.D. Hancock, *J. Chem. Soc., Dalton Trans.* (1983) 1601.
- [13] J.E. Richman, T.J. Atkins, *J. Am. Chem. Soc.* 96 (1974) 2268.
- [14] P. Hoffmann, A. Steinhoff, R. Mattes, *Z. Naturforsch Teil B* 42b (1987) 867.
- [15] J.C.A. Boeyens, S.M. Dobson, R.D. Hancock, *Inorg. Chem.* 24 (1985) 3073.
- [16] A.J. Blake, J.P. Danks, A. Harrison, S. Parsons, P. Schooler, G. Whittaker, M. Schröder, *J. Chem. Soc., Dalton Trans.* (1998) in press.
- [17] A.S. Craig, R. Katak, R.C. Matthews, D. Parker, G. Ferguson, A. Lough, H. Adams, N. Bailey, H. Schneider, *J. Chem. Soc., Perkin Trans 2* (1990) 1523.
- [18] A. McAuley, S. Subramanian, *Inorg. Chem.* 29 (1990) 2830.
- [19] S. Chandrasekhar, A. McAuley, *Inorg. Chem.* 31 (1992) 2234.
- [20] S.A. Ross, Ph. D. thesis, University of Edinburgh, 1994.
- [21] A.J. Blake, J.P. Danks, A. Harrison, W-S. Li, S. Parsons, S.A. Ross, G. Whittaker, M. Schröder, *J. Chem. Soc., Dalton Trans.*, submitted.
- [22] R. Yang, L.J. Zompa, *Inorg. Chem.* 15 (1976) 1499.
- [23] M.R. Squillante, Ph.D. thesis, Tufts University, MA, 1980.
- [24] T.J. Reido, T.A. Kaden, *Helv. Chim. Acta* 62 (1979) 1089.
- [25] E. Kimura, *Topics Curr. Chem.* 128 (1985) 113.
- [26] T. Arishima, K. Hamada, S. Takamoto, *Nippon Kagaku Kaishi* (1973) 1119.
- [27] C.F.G.C. Geraldès, M.C. Alpoim, M.P.M. Marques, A.D. Sherry, M. Singh, *Inorg. Chem.* 24 (1985) 3876.

- [28] R.M. Smith, A.E. Martell, Critical Stability Constants, vol. 2, Amines, Plenum, New York, 1975.
- [29] W. Kläui, H. Otto, W. Eberspach, E. Buchholz, Chem. Ber. 1982 (1922) 115.
- [30] D.M. Wambecke, D. Van de Vondel, E. Claeys, G.G. Herman, A.M. Goeminne, J. Chem. Soc., Dalton Trans. (1992) 829.
- [31] K. Wiegardt, S. Brodka, E.M. Peters, A. Simon, Z. Naturforsch. Teil B 42 (1987) 279.
- [32] R.D. Hancock, S.M. Dobson, J.C.A. Boeyens, Inorg. Chim. Acta 133 (1987) 221.
- [33] D.M. Wambecke, W. Lippens, G.G. Herman, A.M. Goeminne, G.P. Van der Kean, Polyhedron 11 (1992) 2989.
- [34] R.D. Hancock, Pure Appl. Chem. 17 (1978) 2531.
- [35] U. Heinzel, A. Henke, R. Mattes, J. Chem. Soc., Dalton Trans. (1997) 501.
- [36] P. Hoffmann, R. Mattes, Inorg. Chem. 28 (1989) 2092.
- [37] P. Chaudhuri, K. Wiegardt, Y.-H. Tsai, C. Krüger, Inorg. Chem. 23 (1984) 427.
- [38] G. Backes-Dahmann, W. Hermann, K. Wiegardt, J. Weiss, Inorg. Chem. 24 (1985) 485.
- [39] M. Hahn, K. Wiegardt, Inorg. Chem. 23 (1984) 2977.
- [40] G. Backes-Dahmann, K. Wiegardt, Inorg. Chem. 24 (1985) 4049.
- [41] L.R. Gahan, V.A. Grillo, T.W. Hambley, G.R. Hanson, C.J. Hawkins, E.M. Proudfoot, B. Moubaraki, K.S. Murray, D. Wang, Inorg. Chem. 35 (1996) 1044.
- [42] B. N. Figgis, Introduction to Ligand Fields, Wiley, 1966.
- [43] V.A. Grillo, G.R. Hanson, T.W. Hambley, L.R. Gahan, K.S. Murray, B. Moubaraki, J. Chem. Soc., Dalton Trans. (1997) 305.
- [44] T.W. Hambley, L.R. Gahan, Acta Cryst., Sect. C, C42 (1986) 1322.
- [45] L.R. Gahan, T.W. Hambley, G.H. Searle, M.J. Bjerrum, E. Larsen, Inorg. Chim. Acta 47 (1988) 17.
- [46] T.W. Hambley, L.R. Gahan, G.H. Searle, Acta Cryst., Sect. C, C45 (1989) 864.
- [47] L.R. Gahan, T.W. Hambley, A.M. Sargeson, M.R. Snow, Inorg. Chem. 21 (1982) 2699.
- [48] S. Chandrasekhar, A. McAuley, J. Chem. Soc., Dalton Trans. (1992) 2967.
- [49] S. Chandrasekhar, A. McAuley, Inorg. Chem. 31 (1992) 2234.
- [50] L.J. Zompa, T.N. Margulis, Inorg. Chim. Acta 28 (1978) L157.
- [51] W.N. Setzer, C.A. Ogle, G.S. Wilson, R.S. Glass, Inorg. Chem. 22 (1983) 266.
- [52] L.J. Zompa, T.N. Margulis, Inorg. Chim. Acta 45 (1980) L263.
- [53] S. Chandrasekhar, A. McAuley, Inorg. Chem. 31 (1992) 480.
- [54] S.M. Hart, J.C.A. Boeyens, R.D. Hancock, Inorg. Chem. 22 (1983) 982.
- [55] G.J. McDougall, R.D. Hancock, J.C.A. Boeyens, J. Chem. Soc., Dalton Trans. (1978) 1438.
- [56] P. Hoffmann, R. Mattes, Z. Naturforsch. Teil B 43b (1988) 261.
- [57] U. Heinzel, R. Mattes, Inorg. Chim. Acta 194 (1992) 157.
- [58] G. Hunter, A. McAuley, T.W. Whitcombe, Inorg. Chem. 27 (1988) 2634.
- [59] A. J. Blake, R.O. Gould, A. J. Holder, T.I. Hyde, M.O. Odulate, A.J. Lavery, M. Schröder, J. Chem. Soc., Chem. Commun. (1987) 118.
- [60] U. Heinzel, R. Mattes, Polyhedron 10 (1991) 19.
- [61] A.J. Blake, R.D. Crofts, B. DeGroot, M. Schröder, J. Chem. Soc., Dalton Trans. (1993) 485.
- [62] G. Reid, A. J. Blake, T.I. Hyde, M. Schröder, J. Chem. Soc., Chem. Commun. (1989) 1397.
- [63] A.J. Blake, G. Reid, M. Schröder, J. Chem. Soc., Dalton Trans. (1990) 3363.
- [64] G. Reid, M. Schröder, Chem. Soc. Rev. 19 (1990) 239.
- [65] A.J. Blake, A.J. Holder, T.I. Hyde, M. Schröder, J. Chem. Soc., Chem. Commun. (1987) 987.
- [66] A.J. Blake, A.J. Holder, T.I. Hyde, Y. Roberts, A.J. Lavery, M. Schröder, J. Organomet. Chem. 323 (1987) 261.
- [67] A. McAuley, T.W. Whitcombe, Inorg. Chem. 27 (1988) 3090.
- [68] F.V. Lovechio, E.S. Gore, D.H. Busch, J. Am. Chem. Soc. 96 (1974) 3109.
- [69] M.C. Rakowski, M. Rycheck, D.H. Busch, Inorg. Chem. 14 (1975) 1194.
- [70] J.C.A. Boeyens, S.M. Dobson, R.D. Hancock, Inorg. Chem. 24 (1985) 3073.
- [71] L.R. Gahan, C.H.L. Kennard, G. Smith, T.C.W. Mak, Transition Met. Chem. 11 (1986) 465.
- [72] P. Chaudhuri, K. Oder, K. Wiegardt, J. Weiss, J. Reedijk, W. Hinrichs, J. Wood, A. Ozarowski, H. Stratemaier, D. Reinen, Inorg. Chem. 25 (1986) 2951.
- [73] R.D. Bereman, M.R. Churchill, P.M. Schaber, M.I. Winkler, Inorg. Chem. 18 (1979) 3122.
- [74] K. Wasielewski, R. Mattes, Z. Naturforsch. Teil B 47 (1992) 1795.

- [75] U. Heinzel, R. Mattes, *Polyhedron* 11 (1992) 597.
- [76] C. Stockleim, K. Wieghardt, B. Nuber, J. Weiss, U. Flörke, H.-J. Haupt, *J. Chem. Soc., Dalton Trans.* (1991) 1487.
- [77] A.J. Blake, G. Reid, M. Schröder, *Polyhedron* 9 (1990) 2931.
- [78] P. Hoffmann, F.-J. Hermes, R. Mattes, *Z. Naturforsch. Teil B* 43b (1988) 567.
- [79] A. F. Wells, *Structural, Inorganic Chemistry*, S. 444, Clarendon Press, Oxford, 1984.
- [80] D.M. Wambeke, W. Lippens, G.G. Herman, A.M. Goeminne, *Bull. Soc. Chim. Belges* 98 (1989) 307.
- [81] D.M. Wambeke, W. Lippens, G.G. Herman, A.M. Goeminne, D. VandeVondel, G.P. VanderKelen, *Polyhedron* 11 (1992) 1305.
- [82] D.M. Wambeke, W. Lippens, G.G. Herman, A.M. Goeminne, *J. Chem. Soc., Dalton Trans.* (1993) 2017.
- [83] D.M. Wambeke, W. Lippens, G.G. Herman, A.M. Goeminne, *Bull. Soc. Chim. Belges* 98 (1989) 307.
- [84] D. Parker, A.S. Craig, G. Ferguson, A.J. Lough, *Polyhedron* 4 (1989) 2951.
- [85] S.A. Ross, Ph.D. thesis, University of Edinburgh, 1994.
- [86] N.N. Greenwood, A. Earnshaw, *Chemistry of the Elements*, Pergamon Press, Oxford, 1984.
- [87] A.J. Blake, J.P. Danks, A. Harrison, S. Parsons, P. Schooler, G. Whittaker, M. Schröder, *J. Chem. Soc., Dalton Trans.*, in press.
- [88] I.A. Fallis, L.J. Farrugia, N.M. Macdonald, R.D. Peacock, *J. Chem. Soc.Chem. Commun.* (1993) 2759.
- [89] A.J. Blake, S.S.M. Chung, J.P. Danks, W.-S. Li, D.J.E. Spencer, M. Schröder, *J. Chem. Soc. Dalton Trans.*, submitted.
- [90] K. Wasielewski, R. Mattes, *Acta Cryst., Sect. C* C46 (1990) 1826.
- [91] K. Wasielewski, R. Mattes, *Z. Anorg. Allg. Chem.* 619 (1993) 158.
- [92] B. Chak, A. McAuley, T.W. Whitcombe, *Can. J. Chem.* 72 (1994) 1525.
- [93] D.G. Fortier, A. McAuley, *Inorg. Chem.* 28 (1989) 655.
- [94] N.F. Curtis, *J. Chem. Soc.* (1960) 4409.
- [95] E.K. Barefield, F. Wagner, K.D. Hodges, *Inorg. Chem.* 15 (1976) 1370.
- [96] L. Fabbizzi, A. Poggi, P. Zanella, *J. Chem. Soc., Dalton Trans.* (1983) 2191.
- [97] E.K. Barefield, F.W. Wagner, *Inorg. Chem.* 12 (1973) 2435.
- [98] G.C. Silver, W.C. Trogler, *J. Am. Chem. Soc.* 117 (1995) 3983.
- [99] R. Hotzelmann, K. Wieghardt, U. Flörke, H.-J. Haupt, D.C. Weatherburn, J. Bonvoisin, G. Blondin, J.-J. Girerd, *J. Am. Chem. Soc.* 114 (1992) 1681.
- [100] J.R. Hartman, R.L. Rardin, P. Chaudhuri, K. Pohl, K. Wieghardt, B. Nuber, J. Weiss, G.C. Papaefthymiou, S.J. Lippard, *J. Am. Chem. Soc.* 109 (1987) 7387.
- [101] M. Nonoyama, K. Nonoyama, *Transition Met. Chem.* 10 (1985) 382.
- [102] A. Löwe, R. Mattes, K. Wasielewski, *Z. Anorg. Allg. Chem.* 619 (1993) 905.